Stage de fin d'étude - Rapport

# Sensitivity of Fish Stocks Trajectoires to Climate Forcing and Human Exploitation on a Global Scale


**Raphaël BENERRADI**


Année 2023-2024

**Master 2 : Mathématiques pour les Sciences du Vivant (UPS)**
Enseignantes référentes: Sylvie MELEARD, Camille CORON et Sophie DONNET
&
**Cursus Ingénieur CentraleSupélec - 3e année**
Dominante Mathématiques et Data Science
Mention Modélisation Mathématique et Mathémathématiques Financières
Filière Métiers de la Recherche
Référentes pédagogiques: Pauline LAFITTE (mention) et Maria VAKALOPOULOU (filière)

Supervision :

Vasilis DAKOS - Alejandro CANO

Institut des Sciences de l'Evolution-Montpellier

## Abstract

Global fishery resources are of great interest due to potential threats from overfishing and climate change, which could affect marine biodiversity and food security. To better understand the impact of drivers such as fishing pressure and climate change on fish stock dynamics, we explored correlation methods and Empirical Dynamic Modeling (EDM), in particular Convergent Cross-Mapping (CCM), to assess causal relationships between Sea Surface Temperature (SST), harvest rate and fish stock productivity.

Our results show a positive correlation between productivity and harvest rate, consistent with typical fishery trajectories where increasing fishing pressure leads to higher productivity until Maximum Sustainable Yield (MSY) is reached. Fishing pressure was the most commonly identified driver of fish stock productivity in the CCM (56 out of 153 stocks), with the strength of the effect being either positive or negative depending on the stock. The CCM identified causal relationships between SST and productivity for 27 stocks, with a surprisingly positive effect of SST on productivity. The positive effect may reflect potential benefits for some species, or may be explained by methodological limitations that warrant further investigation. Confidence in the causality assessment varied with species traits, particularly for species with faster life histories or experiencing higher fishing pressure, indicating their greater responsiveness to SST changes.

These results provide insights into the causality assessment of drivers of fish stocks from real-world data using EDM methods. Comparisons with other methods, such as Granger causality, could be explored in future work to better understand the limitations and advantages of each causality detection method.

**Résumé**

Les ressources halieutiques mondiales présentent un intérêt considérable en raison des menaces potentielles liées à la surpêche et au changement climatique, qui pourraient avoir un impact sur la biodiversité marine et la sécurité alimentaire. Afin de mieux comprendre l'effet de facteurs tels que la pression de pêche et le changement climatique sur la dynamique des stocks de poissons, nous avons exploré des méthodes de corrélatives et la modélisation dynamique empirique (EDM), en particulier la cartographie croisée convergente (CCM), pour évaluer les relations de cause à effet entre la température de surface de la mer (SST), le taux d'exploitation et la productivité des stocks de poissons.

Nos résultats révèlent une corrélation positive entre la productivité et le taux d'exploitation, ce qui correspond aux trajectoires typiques des pêcheries, où l'augmentation de la pression de pêche entraîne une augmentation de la productivité jusqu'à ce que le rendement maximal durable (MSY) soit atteint. La pression de pêche a été le plus souvent identifiée par la CCM comme un facteur affectant la productivité des stocks de poissons (56 stocks sur 153), avec un effet positif ou négatif selon le stock de poissons. La CCM a identifié des liens de causalité entre la SST et la productivité pour 27 stocks, avec un effet étonnamment positif de la SST sur la productivité. Cet effet positif pourrait refléter les avantages potentiels pour certaines espèces, ou pourrait s'expliquer par les limites de la méthode, ce qui justifie un examen plus approfondi. La confiance dans l'évaluation de la causalité varie en fonction des caractéristiques des espèces, en particulier pour les espèces dont le cycle de vie est plus rapide ou qui subissent une pression de pêche plus élevée. Cela indique une plus grande réactivité aux changements de la SST.

Ces résultats donnent un aperçu de l'évaluation de la causalité des facteurs de changement des stocks de poissons, à partir de données réelles en utilisant des méthodes EDM. Des comparaisons avec d'autres méthodes telles que la causalité de Granger pourraient être explorées dans des travaux futurs afin de mieux comprendre les limites et les avantages de chaque méthode de détection de la causalité.

# Acknowledgements

I would like to warmly thank Vasilis and Alejandro, the very nice supervisors I had during this internship, for guiding me through this project and for their enthusiasm and welcome to ISEM. I would also like to thank Marine Demangeot and Nicolas Meyer from IMAG for their valuable advice and time spent discussing the mathematics. Thanks to Mathieu and Hsiao for their help with the fish and data analysis. And a special thanks to all the members of the BioDICée team that I got to know: the permanents, the post-docs, the PhD students and the interns. I would also like to thank Sylvie Méléard, Camille Coron and Sophie Donnet from M2 MSV, and Pauline Lafitte and Maria Vakalopoulou from CentraleSupélec for supervising me during the internship and this year.

# Contents


**1 Introduction** **1**

1.1 Fisheries and Marine biodiversity . . . . . 1

1.1.1 Stake, status and direct drivers . . . . . 1

1.1.2 Attribution of the drivers . . . . . 1

1.2 Inferring causality . . . . . 2

1.2.1 Interest for ecological data . . . . . 2

1.2.2 Issue with real world data . . . . . 2

1.2.3 Frameworks to approach quasi-causality . . . . . 4

1.3 Granger Causality . . . . . 6

1.4 Empirical Dynamic Modeling . . . . . 7

1.4.1 Mathematical foundations . . . . . 7

1.4.2 Simplex and S-Map Forecasting . . . . . 8

1.4.3 Convergent Cross-Mapping . . . . . 9

1.5 Aim of this work . . . . . 11

**2 Material and Methods** **13**

2.1 Datasets . . . . . 13

2.2 Assessing Links from Correlation . . . . . 16

2.3 Simplex Projection - Estimating the Embedding Dimension . . . . . 17

2.4 S-map - Estimating the nonlinearity . . . . . 22

2.5 Convergent Cross Mapping (CCM) - Inferring Causality . . . . . 24

2.6 Testing the Significance of Causality . . . . . 27

2.7 Confidence and Causal Strength . . . . . 29

2.8 Ecological Patterns in Causality . . . . . 32

**3 Results** **34**

3.1 Assessing Links from Correlation . . . . . 34

3.2 Simplex Projection - Estimating the Embedding Dimension . . . . . 34

3.3 S-map - Estimating the nonlinearity . . . . . 36

3.4 Convergent Cross Mapping (CCM) - Inferring and Characterizing Causality 38

3.5 Ecological Patterns in Causality . . . . . 41

**4 Discussion** **44**

4.1 Correlations between Time Series . . . . . 44

4.2 Causality Assessment . . . . . 44

4.3 Ecological Patterns in Causality . . . . . 46
4.4 Limitations . . . . . 46

**5 Conclusion** **49**
5.1 Variables of Interest . . . . . 49
5.2 Comparison of methods . . . . . 49

**References** **50**

**Supplementary material** **54**

**List of Figures** **63**

# 1 Introduction

## 1.1 Fisheries and Marine biodiversity

### 1.1.1 Stake, status and direct drivers

Fisheries are a significant and increasingly important component of food supply and nutrition. However, fishery resources continue to decline due to a variety of causes, of which fishing pressure is a major one. In 2019, the percentage of overfished fish stocks reached 35.4%, and maximally sustainably fished stocks represented 57.3% of fish stocks (Nations, 2022).

Climate change has and will have impacts on marine biodiversity and ecosystem services - especially food provisioning - through warming temperatures, acidification, deoxygenation, shifts in primary productivity or influxes of particulate organic carbon (POC) (Cooley et al., 2023; Free et al., 2019). These factors lead to poleward shifts in fish and fishery distributions, changes in catch composition, and reductions in fisheries (Cooley et al., 2023). These impacts are associated with geographic patterns, with higher extinction risks in the tropics and invasions in the polar regions (Boyce et al., 2022; Cheung et al., 2013; Jones and Cheung, 2015). Species experience different impacts depending on their thermal niche or life history (Free et al., 2019). Fish and top predators show higher vulnerability and risk to climate change (Boyce et al., 2022; Jones and Cheung, 2018).

Fishing pressure and climate change are also joint impacts, as overfishing has been found to increase the vulnerability of fisheries and reduce their resilience to climate change impacts (Boyce et al., 2022; Cooley et al., 2023; Free et al., 2019).

### 1.1.2 Attribution of the drivers

Identifying the global drivers of fish stocks and their relative importance remains a challenging and difficult task (Bellard et al., 2022). The IPBES Global Assessment provides an estimate of the relative importance of the drivers of global decline in marine ecosystems based on a meta-analysis that identifies direct exploitation as the most important driver, followed by changes in ocean use and climate change (IPBES, 2019). While the attribution methodologies provide outstanding information on the drivers of biodiversity change, they seem to rely mostly on mechanistic models, species distribution models, controlled environment experiments and expert knowledge - e.g. thresholds identified by ecophysiology. These methods allow us to consider a wide range of information through knowledge of the effects involved. However, few studies seem to consider the inference of global causal effects based on data-driven frameworks (Griffith, 2020).

## 1.2 Inferring causality

Identifying drivers means that we aim to infer causality between time series on a global scale based on fish stock assessments. In particular, we investigate causal effects from climate variables to fish stock variables, and from fishing pressure to fish stock variables.

Various definitions of causality - or frameworks for assessing causality - exist, each with its own assumptions and limitations.

Here we consider causality based on *interventions*: if we change one variable (e.g. Sea Surface Temperature), will it have an effect on another variable (e.g. fish stock)? This definition does not consider mechanisms. The goal is not to understand how or why one variable affects another, but to what extent one variable affects another (Dablander et al., 2023).

### 1.2.1 Interest for ecological data

Assessing causality from drivers to ecological variables in real-world data is of interest for several reasons:

- For management: identifying a driver (or a cause of phenomena) allows us to act on that cause to achieve desired outcomes and avoid unintended consequences. This is particularly important for fisheries management, considering drivers such as climate and fishing pressure (Sharp, 1987).
- It is a first step in understanding mechanisms for research purposes: identifying causal relationships can help to study mechanisms by targeting those that can explain the causal relationships.
- There is an increasing amount of global observational data available in ecology. All this recent information can be used to study causal relationships.
- There is a growing interest in understanding the effects of global changes and being able to act to reduce their impacts. This is supported by the Sustainable Development Goals (SDGs), with fisheries being a key component of SDG 2 *Zero Hunger* and SDG 14 *Life Below Water* (United Nations, 2015).

### 1.2.2 Issue with real world data

Assessing causality generally requires experimental data to control for conditions and to replicate the experiment. In this case, correlational methods inform us about potential causal relationships. However, as we aim to study global fisheries and climate variables,

experimental data are unrealistic in this context for practical, ethical and financial reasons. Thus, we only have observational data that represent a single realization of the system, on a global scale, and without controlled conditions. This context poses several challenges:

- Correlations in observational data do not imply causality, or even association between variables. Some examples are reported in the web site spurious correlations, where correlations between two time series appear to be random. One of these examples is treated in this handbook using a causality assessment method presented later in this report (Convergent Cross-Mapping).

- Confounding factors can produce strong correlations that do not correspond to a causal relationship. This is a special case of spurious correlation, which is a priori easier to identify than the general case of spurious correlation due to chance. For example, a confounding factor occurs when a variable Z is a cause of variables X and Y. In this case, X and Y may have a strong linear correlation but no causal relationship. A toy example is presented in Messerli, 2012, which shows a correlation between chocolate consumption and Nobel laureates per country, with explanations being either a spurious correlation or a hidden confounding factor (Prinz, 2020).

- A linear correlation can vary over time between two variables, even if the two variables represent a coupled dynamical system in which each variable influences the future values of the other variable. An example is given in Chang et al., 2017 and Sugihara et al., 2012 with a system exhibiting "mirage correlation" (chaotic behavior that spontaneously exhibits periods of correlation, anticorrelation, or decorrelation):

$$\begin{aligned} X(t+1) &= X(t)[3.8 - 3.8X(t) - 0.02Y(t)] \\ Y(t+1) &= Y(t)[3.5 - 3.5Y(t) - 0.1X(t)] \\ \text{with} \quad & X(0) = 0.4 \quad \text{and} \quad Y(0) = 0.4 \end{aligned} \tag{1}$$

We would like to explore methods that are insensitive to these phenomena to assess causal relationships between time series in the context of real-world data on a global scale.

Note that in the case of observational data, we may prefer to use "quasi-causality" since the term "causality" should be limited to experimental design to qualify what is generally meant in experimental science. For simplicity, however, we will use the term "causality" throughout this report to refer to these relationships between variables in observational data.

### 1.2.3 Frameworks to approach quasi-causality

In this study, we want to assess causality in the case of time series. There are several statistical methods to assess relationships between time series. The Figure 1 is a map of the main methods used in ecology to study time series. We have chosen to classify these methods along two axes to help us understand the aim and principles of the methods. This representation is not universal and not exhaustive, but it provides a global view of statistical methods.

These methods can either consider the time series as a set of independent data, or they can try to account for the temporal structure of the time series - such as the proximity of data points in time, or the direction of time from past to future. We represent this on the horizontal axis in the Figure 1. The methods also provide different information about a possible causal relationship. We decided to classify these methods on an axis from visualization (i.e. just summarizing the information of the time series), to correlation (i.e. providing information about how time series show similar patterns), to "quasi-causality" (i.e. assessing the effect of one variable on another).

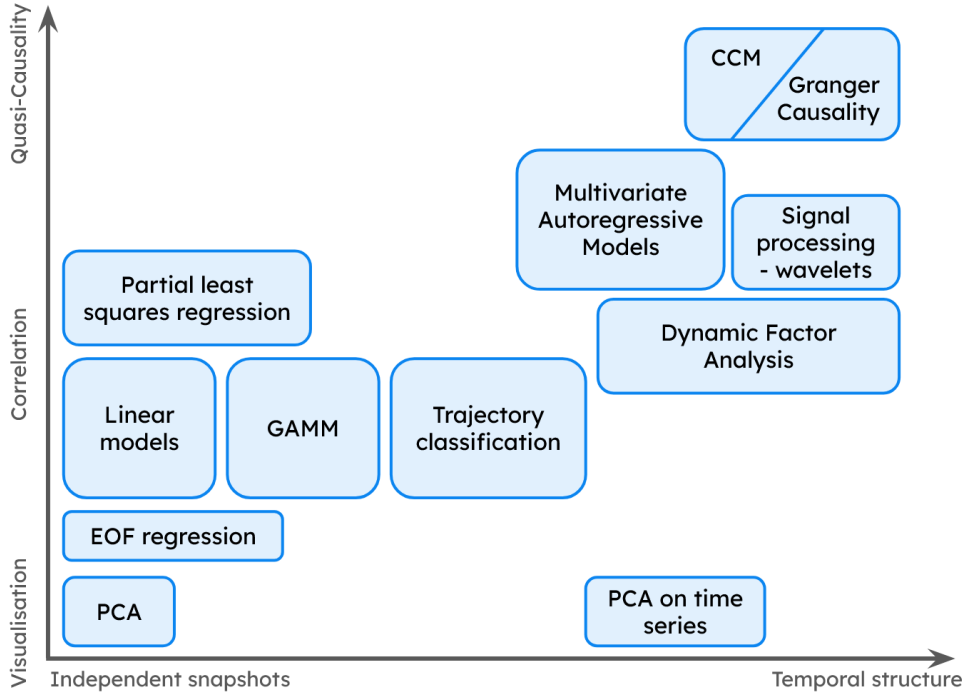


**Figure 1:** Map of the main statistical methods for assessing quasi-causality found in the bibliography.

In the rest of this report, we will focus mainly on Granger Causality and Convergent Cross-Mapping (CCM). Here is a quick overview of the other statistical methods used in ecology, which are presented in the Figure 1:

- PCA: At each time step we have the information of different variables (e.g. climate variable, fishing pressure, fish stock). Thus, each time step is associated with a vector composed of these variables. PCA allows us to identify the main directions of variability of the data in the space with all the variables included in the analysis. We can then visualize patterns of correlations between variables and, finally, some patterns between years. This analysis does not take into account the temporal structure of the time series (de Carvalho-Souza et al., 2021).

- PCA ON TIME SERIES: Instead of applying PCA directly, considering each year as an individual, we start with an interpolation of the time series (e.g. with a basis of splines). Then we apply the PCA to the coefficients of the interpolation of the time series. This allows us to take into account the temporal structure of the time series and to identify patterns of correlations between variables and time.

- EOF REGRESSION: This is a method of reduction of dimensions, similar to the PCA, which is suitable for geographic data. It allows to identify patterns in spatio-temporal data and also to study relationships between variables by defining a model based on some of the variables and the underlying patterns - e.g. linear model (Thorson et al., 2020).

- LINEAR MODELS AND GAMM: Linear models can be used to link variables, considering each year as a realization. This method does not take into account the temporal structure, but it quantifies correlations and effects. GAMMs are an extension of linear models, allowing to consider non-linear relationships between variables.

- TRAJECTORY CLASSIFICATION: Pélissié et al., 2024 proposed a method to classify time series trajectories (linear, quadratic and abrupt) and to quantify parameters on the trajectory (slope, curvature...). This makes it possible to correlate trajectory shapes and parameters between variables (e.g., the relationship between the slope of fish stock over time and the slope of fishing pressure over time). This method is still correlative, but aims to model the temporal structure of the time series.

- PARTIAL LEAST SQUARES REGRESSION: This method allows us to apply a multivariate regression to covariates that have correlations. It is close to a combination of a PCA and a linear regression (Rigal et al., 2023). We can apply this method to the same data as presented in the paragraph on linear models above.

- DYNAMIC FACTOR ANALYSIS: Dynamic factor analysis aims to model each realization of a variable as a linear combination of common trends and a linear combination

of explanatory variables. It allows to take into account the correlation between variables and a temporal structure in the time series - e.g. autocorrelation (Mcowen et al., 2015).

- Multivariate Autoregressive Models: Multivariate Autoregressive Models (or Vector Autoregressive Models) aim to estimate a parametric model that considers the propagation of a noise along the lags to represent an autocorrelation. The method allows flexibility in the definition of the model (e.g. Gompertz model with propagation of a noise along the lags in Mac Nally et al., 2010).

- Signal Processing - Wavelets: These methods involve analyses of frequencies in signals and allows to define a model of relationships between variables (Sarkodie and Owusu, 2023).

Finally, we decide to focus on Granger Causality and Convergent Cross-Mapping (CCM) in the rest of this report. These methods allow to approach quasi-causality and are suitable for ecological time series, as presented below.

## 1.3 Granger Causality

In this framework, introduced in Granger, 1969, a temporal variable $y$ is said to Granger-cause $x$ if the ability to predict $x$ by its lags is improved by adding the lags of $y$ as covariates in the model. This method is based on the idea that if $y$ causes $x$, then the past of $y$ contains information about the present of $x$ - the cause variable explains part of the consequence variable.

In practice, we compare the following two models (Barraquand et al., 2021):

$$\begin{aligned} x(t) &= \alpha_0 + \sum_{i=1}^{p} \alpha_i x(t-i) + \eta_t \quad \text{with} \quad \eta_t \sim \mathcal{N}(0, \sigma_\eta^2) \\ x(t) &= \beta_0 + \sum_{i=1}^{p} \beta_i x(t-i) + \sum_{i=1}^{q} \gamma_i y(t-i) + \epsilon_t \quad \text{with} \quad \epsilon_t \sim \mathcal{N}(0, \sigma_\epsilon^2) \end{aligned} \tag{2}$$

We then test whether the second model - including the lags of $y$ - predicts significantly better than the first model - $x$ alone. This can be done with a test of nested models: a Fisher test with the statistic $F = \frac{(\text{RSS}_1 - \text{RSS}_2)/q}{\text{RSS}_2/(n-p-q-1)}$, where $\text{RSS}_1$ and $\text{RSS}_2$ are the residuals sum of squares of the two models, $q$ is the number of lags of $y$ in the second model, $p$ is the number of lags of $x$ in the models, $n$ is the number of observations for the model ($n$ = timeseries length $- \max(p, q)$ considering the available lags). It is also possible to compare the AIC or BIC of the models and assess causality if the AIC or BIC of the

second model (including the lags of $y$) is lower than the AIC or BIC of the first model. Other tests comparing the log-ratio of the variances estimated in the two models can also be used (Wald test on $\ln\left(\frac{\sigma_\eta^2}{\sigma_\epsilon^2}\right)$ in Barraquand et al., 2021).

Granger Causality is intuitive and relies mainly on comparing correlative models. This makes the method accessible and fairly direct to interpret. Furthermore, the values of the coefficients $\gamma_i$ can provide information about the effect of the causality of a precise lag of $y$ on $x$ - sign and strength of the effect. The method can also be applied to a group of variables. If we also consider a variable $z$, we can test whether $y$ causes $x$ and $z$ by adding the lags of $z$ in the second model presented in Eq. (2).

However, Granger Causality is known to have limitations in the case of non-linear dynamics, especially when the relationship between the variables is not purely stochastic. Indeed, the method is based on linear regressions, which assume that the variables are random variables. The Granger Causality framework may also not be applicable to non-separable variables - i.e. when the information of $y$ is redundant with the time series $x$. Thus, it can become problematic when the variables are part of a dynamical system with coupling between the variables, which is often the case in ecological systems (Sugihara et al., 2012). In addition, this method is parametric and often based on linear models. This can be a limitation when the relationships between variables are non-linear.

Despite all these limitations, Barraquand et al., 2021 found consistent results with Granger Causality in the context of ecological time series, simulated non-linear dynamics, and real-world data. We did not apply Granger Causality in this report, but it will be part of future work.

## 1.4 Empirical Dynamic Modeling

To avoid the limitations of Granger Causality mentioned in the previous section, we decided to focus on Empirical Dynamic Modeling (EDM) and Convergent Cross-Mapping (CCM) in this report. These methods are nonparametric and suitable for fish stock analysis (Sugihara et al., 2012).

### 1.4.1 Mathematical foundations

Empirical Dynamic Modeling (EDM) is a framework for studying dynamical systems with nonparametric methods. It is mainly based on Taken's theorem, presented in Takens, 2006 and stated in Box 1.4.1. This theorem focuses on the attractor of a dynamical system, and an approximation of this manifold from the lags of a single variable of the dynamics.

**Taken's Theorem, 1981 - for discrete-time dynamics (rewritten from Wikipedia)**

Let $M$ be the manifold of the dynamics of the time series $x$. The dynamics is given by a smooth map $f : M \to M$ (i.e. $x(t+1) = f(x(t))$). Let us assume that the dynamics $f$ has a strange attractor $A \subset M$ (i.e. a fractal structure, especially common in chaotic dynamics) of dimension $d_A$. Thus, $A$ can be embedded in a $k$-dimensional Euclidean space, with $k > 2d_A$ (i.e. there exists a diffeomorphism with full rank derivatives, that maps $A$ to $\mathbb{R}^k$).
Let $\alpha : M \to \mathbb{R}$ be a twice-differentiable observation function with full rank derivatives and no special symmetries in its components (e.g. projection onto one of the variables of the system).
The Taken's theorem states that

$$\begin{aligned} \varphi : A &\longrightarrow \mathbb{R}^k \\ u &\longmapsto \big(\alpha(u)\ ,\ \alpha(f(u))\ ,\ \dots\ ,\ \alpha(f^{k-1}(u))\big) \end{aligned}$$

is an embedding (i.e. a diffeomorphism from a differentiable manifold to a submanifold, whose differential is everywhere injective).

A simple way to interpret this theorem is that the shape in space of the lags of a single variable ($\varphi(A)$ in the Box 1.4.1) is similar to the shape of the complete state space of the dynamics ($A$ in the Box 1.4.1). This is shown for the Lorenz attractor in the animation here (Sugihara et al., 2012).

This theorem is used to approximate the complete system manifold from the information of a single variable. This approximation is the basis in EDM for forecasting one variable and for predicting other variables (used to evaluate relationships between variables, especially causality).

### 1.4.2 Simplex and S-Map Forecasting

Based on Taken's theorem, the lags of a single variable follow a manifold in an embedding space of the lags of that variable. Since the initial manifold is smooth ($f$ is smooth in the Box 1.4.1) and the embedding is smooth ($\varphi$ is a diffeomorphism in the Box 1.4.1), the dynamics and the manifold in the embedding Euclidean space is also smooth ($\varphi \circ f$). Then, if we want to forecast the variable at a given time ($\alpha(f^k(u^*))$ after observing $\alpha(f^{k-1}(u^*))$), we can use some observed points in this lag space that are close to the point of interest (points close to $\big(\alpha(u^*)\ ,\ \alpha(f(u^*))\ ,\ \dots\ ,\ \alpha(f^{k-1}(u^*))\big)$ noted $\big(\alpha(u_{near})\ ,\ \alpha(f(u_{near}))\ ,\ \dots\ ,\ \alpha(f^{k-1}(u_{near}))\big)$), in order to predict the next step

of interest of the variable depending on the next step of the observed points ($\alpha(f^k(u^*))$ predicted close to $\alpha(f^k(u_{near}))$).

There are two main methods to predict based on the observed points ($u_{near}$): the Simplex projection uses the nearest neighbors, the S-map forecasting uses an exponential decay to weight the points in the embedding space (Munch et al., 2023). These methods are described in detail in the sections 2.3 and 2.4.

The Simplex and S-map forecasting are nonparametric methods, and are suitable for nonlinear dynamics. They allow forecasting, but here, we will use it to find the best embedding dimension, i.e. to approach the $k$ mentioned in Box 1.4.1 (later referred to as $E$), and to estimate the degree of nonlinearity of the dynamics (details in 2.4). The embedding dimension is the number of lags of the variable needed to approximate the manifold of the dynamics. It is a key parameter in the EDM, and especially in the Convergent Cross-Mapping (CCM), which we will introduce below. In addition, the S-map forecasting informs us about the nonlinearity of the dynamics. The nonlinearity can justify the use of EDM methods - which are suitable for nonlinear dynamics compared to other methods such as Granger Causality (Sugihara et al., 2012).

### 1.4.3 Convergent Cross-Mapping

The Convergent Cross-Mapping (CCM) is an EDM method that aims to detect causality between variables. In this framework, a variable $y$ is said to cause the variable $x$ if $y$ and $x$ interact in the same dynamical system (i.e. they share a common attractor) and past values of $y$ affect the future values of $x$ (e.g. $\frac{\partial y}{\partial t}$ depends on $x$). A typical example is presented with discrete-time observations in Sugihara et al., 2012:

$$\begin{aligned} x(t+1) &= x(t)\left[r_x - r_x x(t) - \beta_{x,y} y(t)\right] \\ y(t+1) &= y(t)\left[r_y - r_y y(t) - \beta_{y,x} x(t)\right] \end{aligned} \tag{3}$$

In Eq. (3), $r_x$ and $r_y$ are the growth rates of $x$ and $y$, $\beta_{x,y}$ and $\beta_{y,x}$ are the coupling coefficients.

One of the advantages of the CCM is that it is suitable for systems that are not purely stochastic such as systems with an underlying dynamics. It also allows us to study nonlinear dynamics, especially due to the fact that it is a nonparametric method. Furthermore, it is applicable to non-separable systems, that is when the information of $y$ is redundant with the time series $x$. This is often the case in dynamical systems. These situations can be problematic for Granger Causality methods (Sugihara et al., 2012).

In Eq. (3), if $\beta_{x,y} \neq 0$ and $\beta_{y,x} = 0$, $y$ causes $x$ but $x$ does not cause $y$. The system

becomes:

$$\begin{aligned} x(t+1) &= x(t)\left[r_x - r_x x(t) - \beta_{x,y} y(t)\right] \\ y(t+1) &= y(t)\left[r_y - r_y y(t)\right] \end{aligned} \tag{4}$$

and then, if we assume that $x(t) \neq 0$, it can be rewritten as follows,

$$\begin{aligned} y(t) &= \frac{x(t+1)}{\beta_{x,y} x(t)} - \frac{r_x}{\beta_{x,y}} + \frac{r_x}{\beta_{x,y}} x(t) \\ y(t+1) &= y(t)\left[r_y - r_y y(t)\right] \end{aligned} \tag{5}$$

and we get

$$y(t+1) = r_y \left( \frac{x(t+1)}{\beta_{x,y} x(t)} - \frac{r_x}{\beta_{x,y}} + \frac{r_x}{\beta_{x,y}} x(t) \right) - r_y \left( \frac{x(t+1)}{\beta_{x,y} x(t)} - \frac{r_x}{\beta_{x,y}} + \frac{r_x}{\beta_{x,y}} x(t) \right)^2 \tag{6}$$

Here, in a simple purely deterministic example, we see that $y$ is determined by the lags of $x$. More generally in the CCM, in order to assess whether $y$ causes $x$, we will try to check whether $y$ can be predicted from the lags of $x$. This general case relies on the Taken's theorem presented in Takens, 2006 (see the Box 1.4.1), with its extensions in Deyle and Sugihara, 2011. These theorems provide arguments on the manifold of the dynamics, and mappings of this manifold from the lags of a single variable of the dynamics. The prediction is based on an attractor reconstruction of the manifold of $y$ from a manifold in the embedding space of the lags of the variable $x$. The Figure 2 shows this reconstruction for the example of the Lorenz attractor (figure from Sugihara et al., 2012).

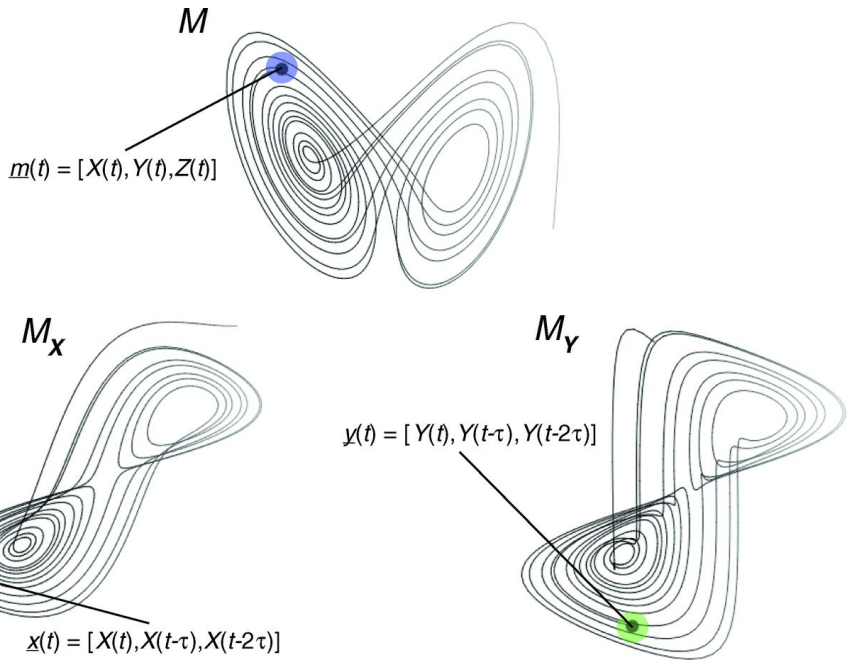


**Figure 2:** Embedding and manifold approximation used in the CCM for the Lorenz attractor. $M$ is the manifold of the complete dynamics, $M_x$ and $M_y$ are the approximations based on the lags of the single variables $x$ and $y$. (Figure from Sugihara et al., 2012)

Even if this direction of prediction may be contrary to intuition and to Granger Causality (from $x$ to $y$ to estimate causality from $y$ to $x$), when we have a causal relationship in a dynamical system, the past of the *consequence* variable contains information about the present of the *cause* variable. This is mainly due to the fact that the dynamical system generates a coupling between the variables and that the variables are not purely stochastic (which is an assumption in Granger Causality that may not hold).

We can note that the relationship between $x$ and $y$ in Eq. (3) can exhibit - for certain values of the parameters - a chaotic behavior, which spontaneously exhibits long periods of correlation, anti-correlation or decorrelation. Thus, Granger Causality has limitations in this type of system, especially because it relies on correlative models. On the contrary, CCM is suitable for this example. Furthermore, EDM and CCM are known to be suitable for ecological time series, especially fish stocks (Sugihara et al., 2012).

## 1.5 Aim of this work

In this report, we examine the sensitivity of fish stocks to drivers, specifically climate change and fishing pressure. We aim to identify potential causal relationships between these drivers and fish stocks, and to quantify the relative importance of each driver. To this end, we use causal assessment frameworks, with a focus on Empirical Dynamic Modeling. We also focus on functional traits and management status and trends to reveal

ecological patterns associated with the effects of drivers on fish stocks. This study aims to address the following questions:

1. Are there causal effects of climate change (especially Sea Surface Temperature) and fishing pressure on fish stocks, to assess whether we can identify such an effect?
2. Can we quantify the relative magnitude of the causal relationships, for the drivers and depending on the fish stock?
3. Are there ecological patterns - functional traits, historical fishing pressure - that influence the intensity of the effect of the drivers?

The following section presents the data and the methods used to assess a causal relationship, in particular correlative methods and Empirical Dynamic Modeling (including parameterization and checks, from Simplex projection to S-map to Convergent Cross-Mapping and strength assessment). This section also includes the methods used to analyze the ecological pattern. Then, we present the results obtained by applying the methods. Finally, we discuss the results and limitations of the methods, and conclude with some perspectives for future work.

# 2 Material and Methods

## 2.1 Datasets

We used the RAM Legacy Stock Assessment Database version v4.64 (RAMLDB) which provides fishery-related data for 1435 commercially exploited marine fish and invertebrate stocks (Ricard et al., 2012). This dataset provides the annual time series of total biomass, total catch and harvest rate.

Based on the total biomass and total catch, we computed the time series of the surplus of productivity for each year for each stock. The surplus of productivity (or later refered as productivity) quantifies how much the biomass has evolved within the stock, removing the part of the fishing in this change. Productivity is mainly due to growth of the individuals, reproduction and mortality (except fishing mortality). It is defined as $\text{Prod}(t) = \text{TB}(t+1) - \text{TB}(t+1) + \text{TC}(t)$ (Hilborn, 2001; Vert-Pre et al., 2013) with details in Figure 3. This formula was applied to the variables `TBbest` and `TCbest` in the RAMLDB for each stock. In this report, productivity is the variable that represents the fish stock.

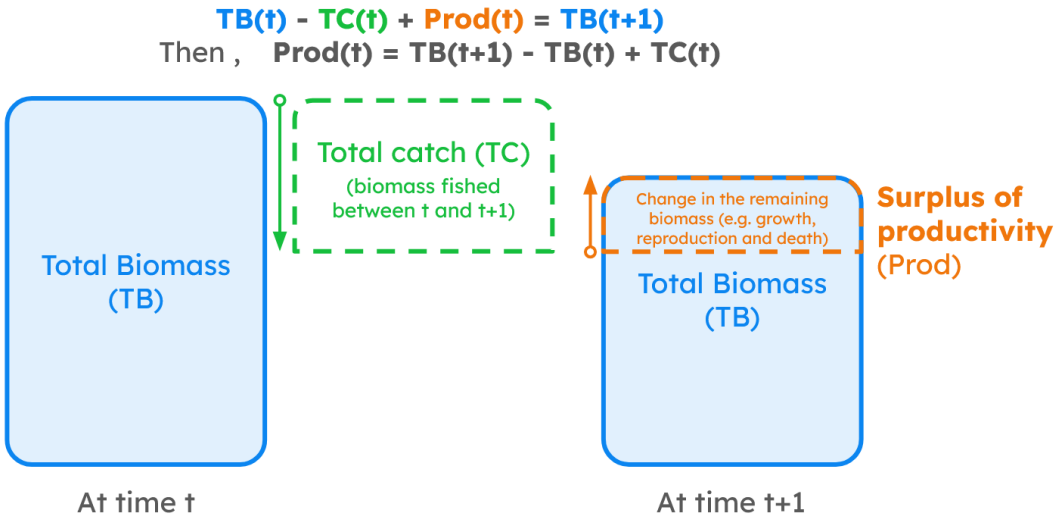


**Figure 3:** Diagram representing the definition of the surplus of productivity based on biomass and catch. In this example, the surplus of productivity is positive and biomass has decreased.

We considered the harvest rate to be the variable that quantifies the fishing pressure on fish stocks. In the RAMLDB, harvest rate refers to either exploitation rate or fishing mortality. We use the harvest rate normalized by the harvest rate at the management target reference point ($U_{MSY}$). Thus, a fish stock with $U = 1$ is at the management target reference point, a fish stock with $U > 1$ is overfished with respect to the harvest

rate, and underfished if $U < 1$. The normalized harvest rate is available in the variable `UdivUmgtpref` in the RAMLDB.

Finally, to obtain a climate variable corresponding to each stock, we collected the geographic boundaries of the stocks in the RAMLDB, available at Christopher Free's website. The boundaries allow to extract climate variables from high resolution global datasets along time and to match these climate variables with the stock boundaries to get the climate variable for each stock along time.

We decided to use Sea Surface Temperature (SST) as the climate variable. This variable is available at high resolution and is expected to have an effect on fish stocks (see section 1.1). We used the Met Office HadISST1 dataset to get the global SST data along time (Rayner et al., 2003 and available here). SST data are available at daily time resolution, but we use only the annual averages to match the time resolution of the fish stock data. Then, for each stock, for each year, the SST is calculated as the average within the stock boundary of the annual SST average. The Figure 4 shows the SST data and the boundary of the stock MORWONGESE within which we compute the average of the SST. Note that the MORWONGESE stock will be used throughout the rest of the report to illustrate the analysis. This stock is the east-southeast population of the Jackass morwong, distributed near Australia.

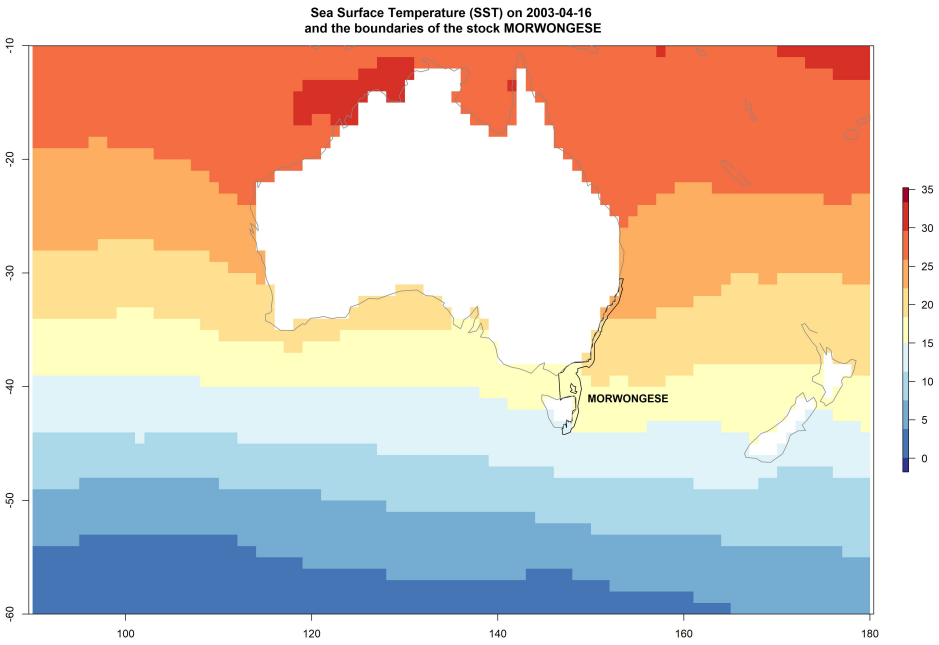


**Figure 4:** Sea Surface Temperature (SST) data with the boundary of the MORWONGESE stock (in black, on the southeast coast of Australia). The colors represent the SST data from April 16, 2003.

Finally, we have 302 marine fish and invertebrate stocks with the variables of produc-

tivity, normalized harvest rate, and SST. The durations of the time series for each stock are available in Supplementary Materials Figure 29.

Before applying the analysis, we standardize the data to obtain time series within ranges of similar order of magnitude, especially between stocks. The SST is standardized within each stock using a Z-score (centered and scaled). Then, for each stock, productivity is divided by the average of the stock's total biomass along the time series (Essington et al., 2015). Total biomass is comparable to productivity, and this standardization provides something like the rate of average biomass produced during the year. Finally, the harvest rate is left as it is, as it is already normalized by the harvest rate at the management target reference point.

The three time series are shown in the Figure 5 for the stock MORWONGESE. The three variables are shown for all stocks in the Figure 6.

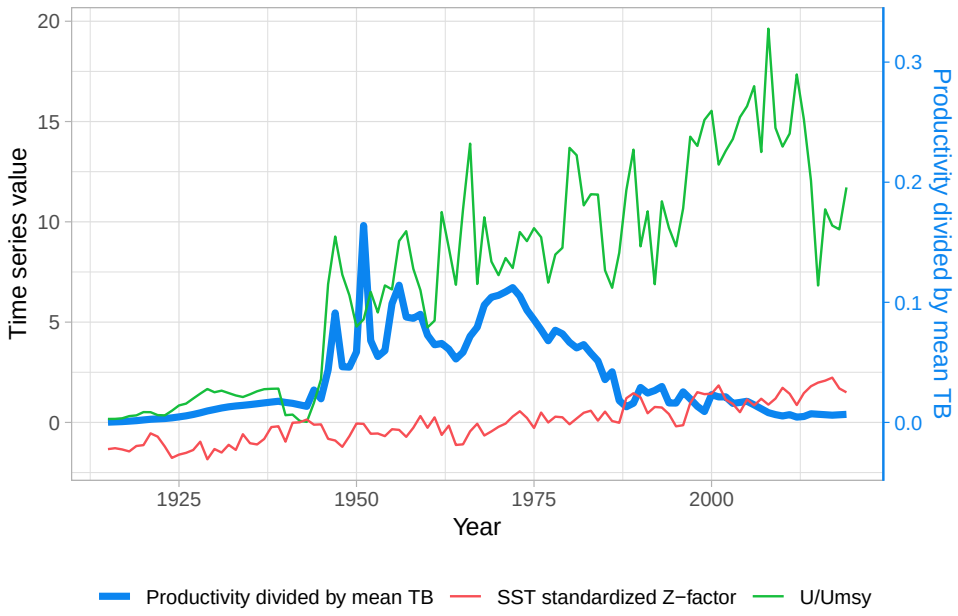


**Figure 5:** Example of the three time series for the stock MORWONGESE.

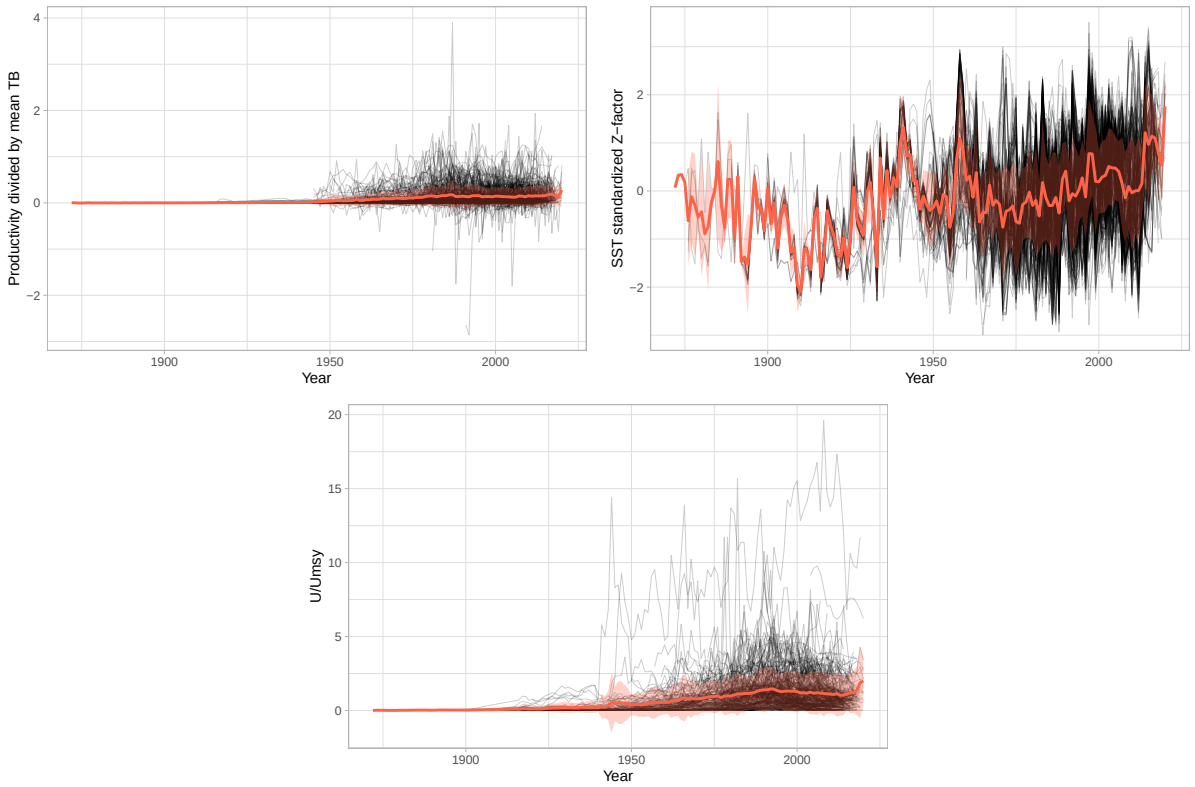


**Figure 6:** Time series for all stocks in the dark curves. The red curves are the mean among the stocks for each year. The red bands represent one standard deviation around the mean among the stocks for each year. Upper left: productivity, upper right: SST, bottom: harvest rate.

As expected, the time series are autocorrelated, which encourages us to use methods that can take into account the temporal structure of the data. The autocorrelation of the time series is shown in the Supplementary Materials Figure 30.

## 2.2 Assessing Links from Correlation

A first approach to assess relationships between time series is to use correlations. For each stock, we computed the Spearman correlation between each pair of variables. We also computed the Spearman correlation between each pair of variables including all stocks indifferently (correlation computed on the concatenation of all time series). For example, for productivity and SST, we get the correlations between Prod($t$) and SST($t$). This refers to correlations with a lag of 0. We also computed the correlations with a lag of $l$, as the correlations between Prod($t + l$) and SST($t$). This can provide information about correlations between variables with a delay. We computed the Spearman correlations for lags between -4 and 4.

## 2.3 Simplex Projection - Estimating the Embedding Dimension

The simplex projection is an EDM method that will be useful in our process to obtain information about the embedding dimension that best represents the dynamics of the system. It is the first step of our process, which will include: estimating the embedding dimension (simplex projection), estimating the nonlinearity (S-map forecasting), estimating the causality (CCM based on the optimal embedding dimension), quantifying the strength of the causality (approximating the dynamics using the estimated nonlinearity).

We consider the time series $x$ with $n$ observations at regular time intervals $t \in \{t_1, \dots, t_n\}$ (i.e. with $t_{i+1} - t_i$ constant for $i \in \{1, \dots, n-1\}$). In our case, $x$ is the productivity, the SST or the harvest rate, and $t$ is a year.

Let $E \in \mathbb{N}^*$ be the embedding dimension (to be determined later). We consider the embedding space defined as an $E$-dimensional space of lags of the time series, containing the following vectors: $\underline{\boldsymbol{X}}(t) = (x(t-(E-1)\tau)\ ,\ x(t-(E-2)\tau)\ ,\ \dots\ ,\ x(t-\tau)\ ,\ x(t))$ where $\tau$ is a multiple of the constant time interval. In our case, we set $\tau$ to one time interval (1 year) to keep as many data points as possible.

The simplex projection aims at predicting the next step of a time series from this embedding space, based on arguments of continuity in the path of the attractor in the embedding space (Takens, 2006). Let us try to predict the value $x(t^*+1)$ for a given time $t^*$. We call this prediction $\hat{x}(t^*+1)$. We consider the $E+1$ nearest neighbors of the point $\underline{\boldsymbol{X}}(t^*) = (x(t^*-(E-1)\tau)\ ,\ x(t^*-(E-2)\tau)\ ,\ \dots\ ,\ x(t^*-\tau)\ ,\ x(t^*))$ in the embedding space, for the Euclidean norm (norm 2). Selecting $E+1$ nearest neighbors allows the current point $\underline{\boldsymbol{X}}(t^*)$ to be inside the simplex formed by the $E+1$ nearest neighbors being the vertices (in principle but not necessarily realized).

Let $\underline{\boldsymbol{X}}(t^j)$ for each $j \in \{1, \dots, E+1\}$ be the $E+1$ nearest neighbors of $\underline{\boldsymbol{X}}(t^*)$ in the embedding space. We consider the next step of the time series for each of the $E+1$ nearest neighbors, i.e. $x(t^j+1)$ for $j \in \{1, \dots, E+1\}$. The prediction $\hat{x}(t^*+1)$ is then computed as the weighted average of the next step of the nearest neighbors, with weights decreasing exponentially with the distance to $\underline{\boldsymbol{X}}(t^*)$:

$$\hat{x}(t^*+1) = \sum_{j=1}^{E+1} w_j x(t^j+1) \quad \text{with } w_j = \frac{u_j}{\sum_{k=1}^{E+1} u_k} \text{ and } u_i = \exp\left\{ -\frac{\left\|\underline{\boldsymbol{X}}(t^i) - \underline{\boldsymbol{X}}(t^*)\right\|}{\left\|\underline{\boldsymbol{X}}(t^1) - \underline{\boldsymbol{X}}(t^*)\right\|} \right\} \tag{7}$$

The Figure 7 illustrates the simplex projection for the stock MORWONGESE for the productivity in the year 1963 (i.e. $t^* = 1962$).

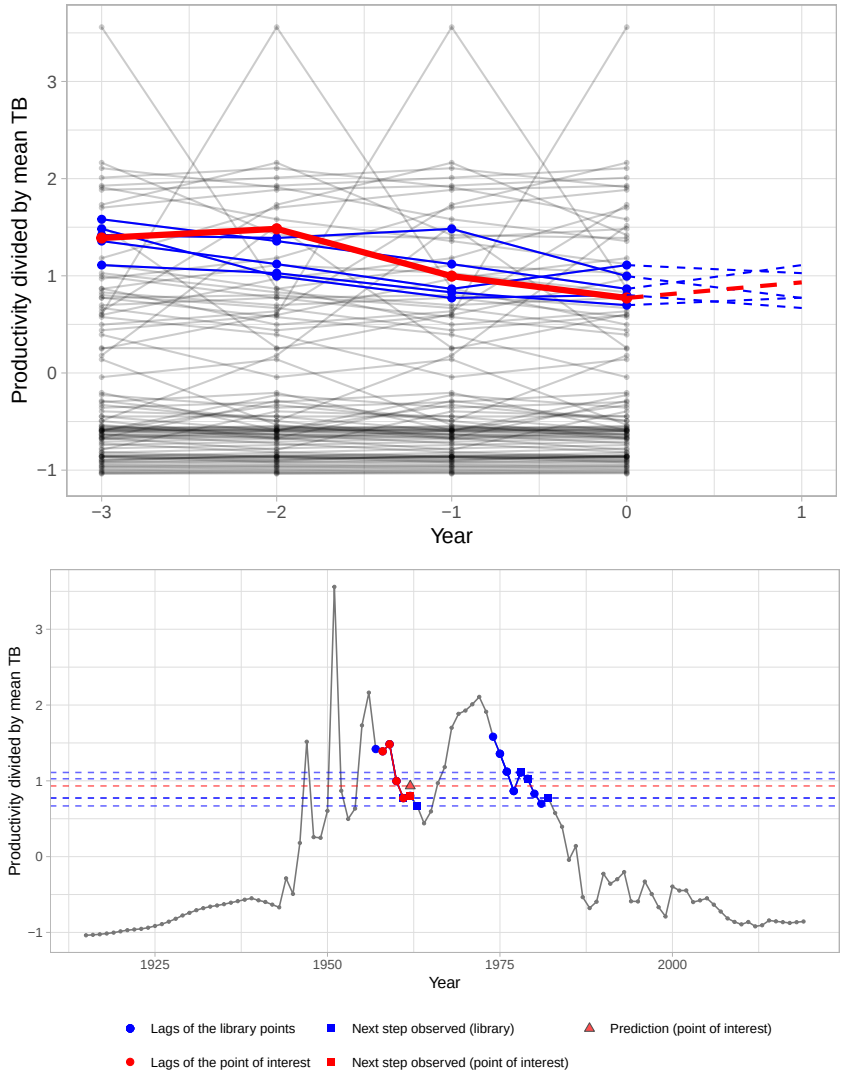


**Figure 7:** Visualization of the simplex projection for the productivity of the stock MORWONGESE. The figure above is a visualization of each point $\underline{\boldsymbol{X}}(t)$ in the embedding space, here with $E = 4$. Each curve represents the 4 coordinates in the embedding space for a given time $t$: $x(t-3)$, $x(t-2)$, $x(t-1)$ and $x(t)$. The red curve represents the vector $\underline{\boldsymbol{X}}(t^*)$ for the year 1962. The blue curves represent the $E+1 = 5$ nearest neighbors of $\underline{\boldsymbol{X}}(t^*)$ in the embedding space. The figure below is a visualization of the time series, with the year 1962 and its 3 lags in red, and the nearest neighbors composed by 4 consecutive time points in blue. The dashed lines in blue for both figures represent the next observed values for each nearest neighbor. Then, the prediction for the year 1963 in red is computed as defined above, with a weighted average of the next observed values of the nearest neighbors. Points may overlap in this figure.

Now that we know how to predict the next step of a time series from the embedding space, for a given year, we can apply this simplex projection to each time point. Then, for each time point, we know the observed value, and we get the prediction from the simplex projection. We compute the forecasting skill ($\rho$) for the entire time series, as the

correlation between the observed values and the predicted values for all points in the time series.

The simplex projection needed to define the embedding dimension $E$. We can apply the simplex projection for different values of $E$ and compute the forecasting skill for each value of $E$ (Figure 8). We decided to use the simplex projection for $E$ between 1 and 15.

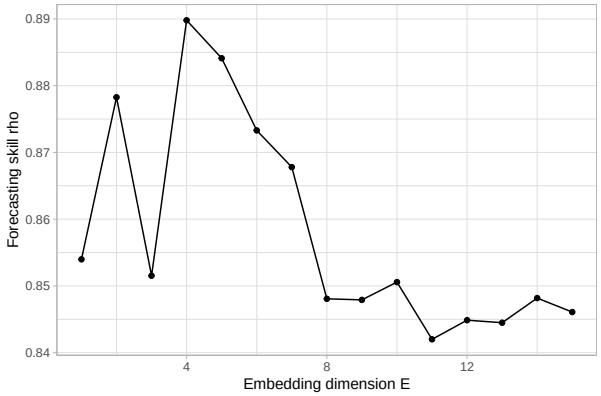


**Figure 8:** Forecasting skill in the simplex projection depending on the embedding dimension for the productivity of the stock MORWONGESE

We applied this process to all the stocks. The visualization of the forecasting skill as a function of the embedding dimension for all stocks is shown in Figure 9.

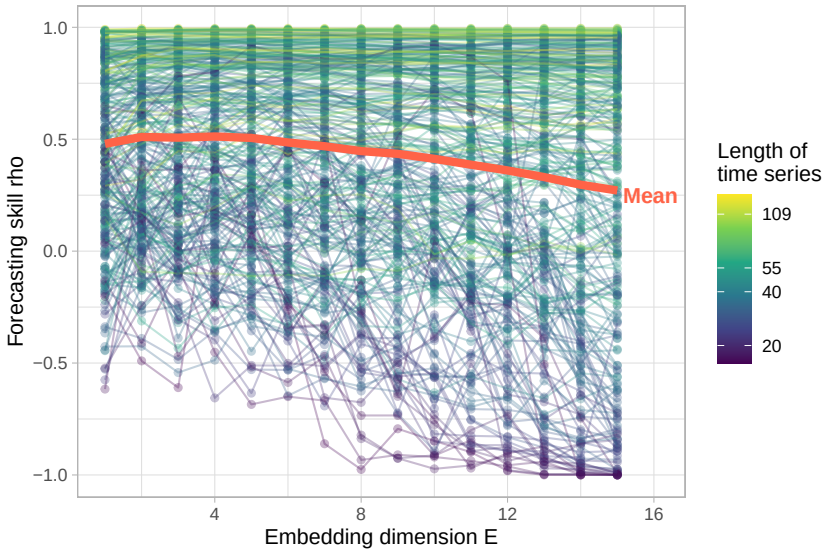


**Figure 9:** Forecasting skill in the simplex projection depending on the embedding dimension for the productivity for all the stocks

The aim of the simplex projection was to find the optimal embedding dimension $E$ that best represents the dynamics of the system. We chose the embedding dimension that maximizes the forecasting skill while remaining low enough (parsimonious choice). To do

this, we considered the smallest $E$ in the top 20% of the range of the forecasting skills.

Surprisingly, we found that the forecasting skill was sometimes negative (prediction is the opposite of the observation). This was especially true for short time series and high embedding dimensions. Indeed, the number of nearest neighbor candidates is limited by the number of data points. Thus, the number of different predictions that can be computed is small, and the prediction may be very sensitive and not reliable. Even worse, the forecasting skill was sometimes negative at the optimal embedding dimension defined above, which we should consider as the optimal one to represent the dynamical system.

As previously done for fish stocks, we will only kept time series with at least 40 time points to apply EDM (Pierre et al., 2018). Furthermore, forecasting skills at the optimal embedding dimension that are negative are not reliable. We did not consider such stocks in the following analysis. The Figure 10 shows these filters applied: time series with less than 40 time points (in red), and forecasting skills at the optimal dimension that are negative (on the left of the vertical dashed line).

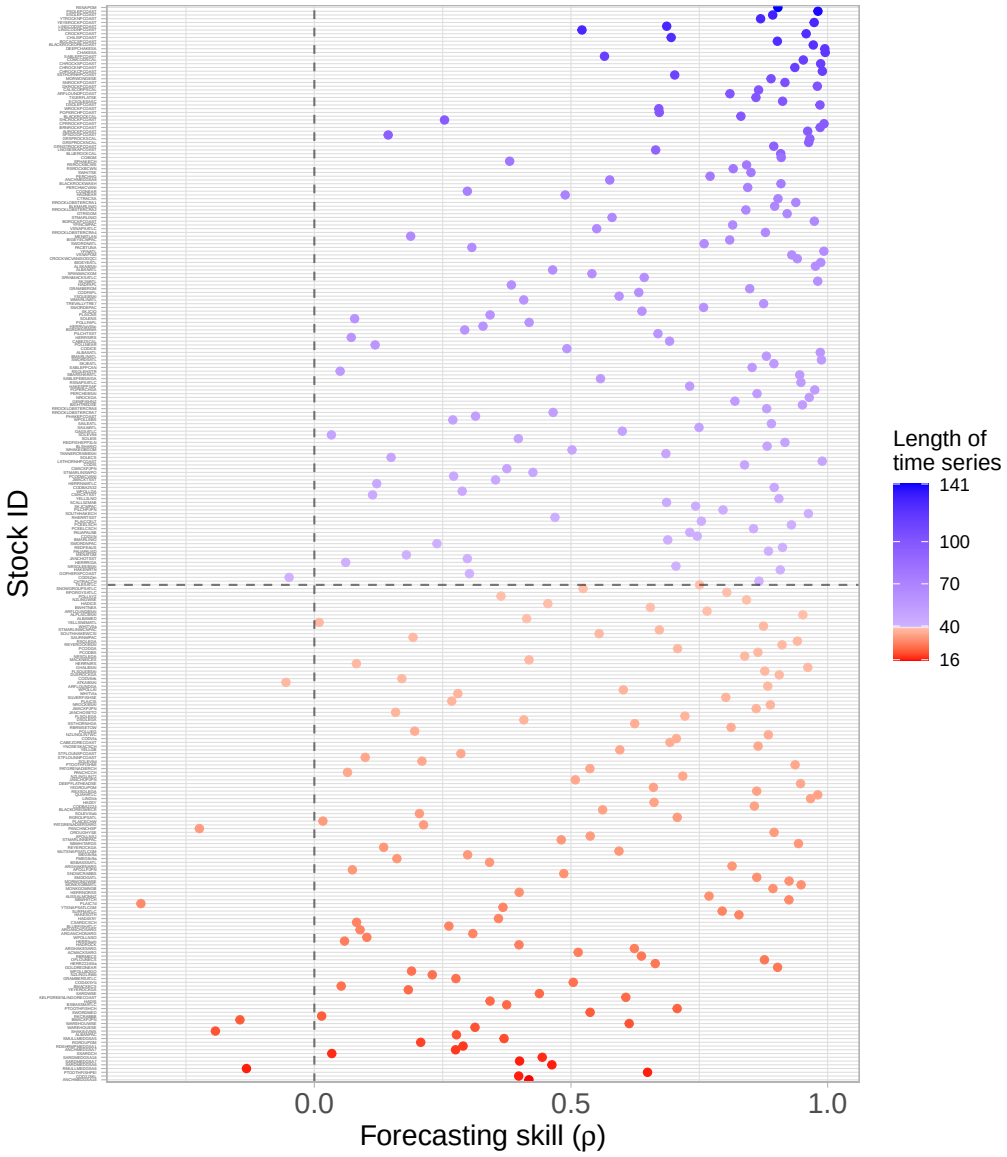


**Figure 10:** Forecasting skill in the simplex projection at the optimal embedding dimension for the productivity for each stock. The vertical dashed line represents the cutoff at $\rho = 0$. The horizontal dashed line represents the cutoff at 40 time points. The red dots are the stocks with less than 40 time points, and the blue dots are the stocks with more than 40 time points.

With this process, we now have the time series that are relevant to Empirical Dynamic Modeling methods, and their associated optimal embedding dimension.

In addition, we can check that the time series are not purely random and that the simplex projection gives a consistent result. In the Eq. (7) we have predicted the next step $\hat{x}(t^* + 1)$. The method remains applicable for any time horizon $h$ for prediction, i.e. predicting the value $\hat{x}(t^* + h)$ with the weighted average of the values of the nearest neighbors $\hat{x}(t^j + h)$. For a given embedding dimension (e.g. the previously obtained

optimal $E$), we applied the simplex projection and obtained a forecasting skill $\rho$ for each time horizon $h$. If the EDM method is consistent, we expect the forecasting skill to decrease as the time horizon for the forecast increases. Even for periodic time series or dynamics, the information of periodicity should be induced by the embedding dimension, and the forecasting skill for this optimal embedding dimension should decrease with the time horizon for prediction. We can compute the forecasting skill for each time horizon and check whether the forecasting skill decreases as the time horizon increases. If the signal is purely random, the forecasting skill should remain stable with time horizon. This result is shown for the productivity of the stock MORWONGESE in the Figure 11.

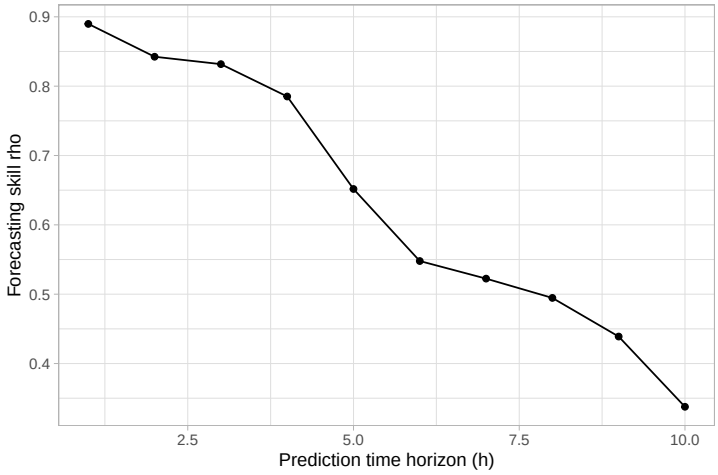


**Figure 11:** Forecasting skill in the simplex projection depending on the time horizon of prediction for the productivity of the stock MORWONGESE

## 2.4 S-map - Estimating the nonlinearity

The second step includes the S-map, which informs us about the degree of nonlinearity of the system dynamics. Nonlinearity here refers to the behavior of the attractor and to the fact that if the points $\underline{\boldsymbol{X}}(t_k)$ and $\underline{\boldsymbol{X}}(t_l)$ are far apart in the embedding space, they will have very different future values $x(t_k+1)$ and $x(t_l+1)$. When time series have nonlinear dynamics, this supports the relevance of using the EDM framework.

S-map is similar to the simplex projection (see Eq. (7)), except that we consider all points in the embedding space (the considered points are called library points), not just the nearest neighbors. The prediction is then computed as the weighted average of the next step of all library points, with the weights decreasing exponentially with the distance to the point of interest, using a parameter that controls the exponential decay: the nonlinearity parameter $\theta$. Let $t_i$ be the times of all library points in the embedding space (by default, all times $t_i$ for $i \in \{1, \ldots, n\}$). The prediction $\hat{x}(t^*+1)$ for a given

time $t^*$ is then computed as:

$$\begin{aligned} &\hat{x}(t^*+1) = \sum_{i=1}^{n} \tilde{w}_i x(t_i+1) \\ &\text{with } \tilde{w}_i = \exp\left\{-\theta \frac{\|\underline{\boldsymbol{X}}(t_i) - \underline{\boldsymbol{X}}(t^*)\|}{D}\right\} \text{ and } D = \frac{1}{n}\sum_{k=1}^{n} \|\underline{\boldsymbol{X}}(t_k) - \underline{\boldsymbol{X}}(t^*)\| \end{aligned} \tag{8}$$

When $\theta = 0$, all weights $\tilde{w}_i$ are equal to 1, so all points in the embedding space are considered equally for prediction. As $\theta$ increases, the weights decrease exponentially with the distance to the point of interest, so the prediction is more influenced by the nearest neighbors in the embedding space. The nonlinearity parameter $\theta$ controls the exponential decay of the weights, and is thus a proxy for the nonlinearity of the dynamics.

As in the simplex projection, we know the observed values and compare them with the prediction from the S-map to get a forecasting skill, also defined as the correlation between the observed and predicted values for all points in the time series. We can run the S-map for different values of the nonlinearity parameter $\theta$ and compute the forecasting skill for each value of $\theta$ (Figure 12).

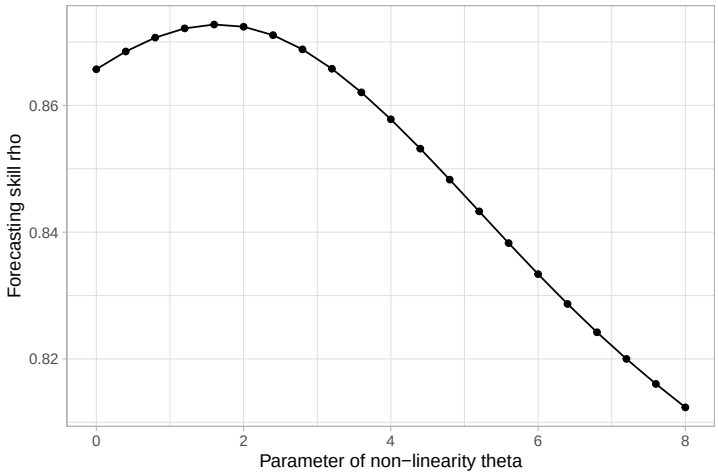


**Figure 12:** Forecasting skill in the S-map at optimal $E = 4$ as a function of the nonlinearity parameter $\theta$ for the productivity of the stock MORWONGESE

For example, for the productivity of the stock MORWONGESE, the forecasting skill is maximized for $\theta = 1.6$ when $E$ is at its optimal embedding dimension $E = 4$. It is also possible to run it for different values of $E$ and $\theta$ and compute the forecasting skill for each combination of $E$ and $\theta$. These results are shown in the Figure 13 for productivity for the stock MORWONGESE.

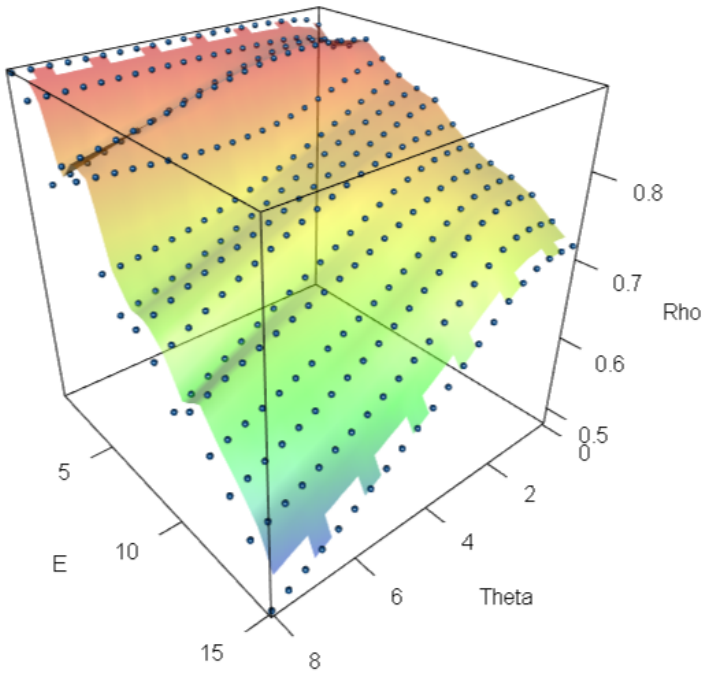


**Figure 13:** Forecasting skill in the S-map depending on the nonlinearity parameter $\theta$ and the embedding dimension $E$ for the productivity of the stock MORWONGESE

## 2.5 Convergent Cross Mapping (CCM) - Inferring Causality

The purpose of CCM is to assess the causality between two time series. In order to test all possible causal relationships, we applied this method to each pair of variables: 6 pairs to test the 2 directions of causality between the 3 variables (productivity, SST, and harvest rate).

As presented in section 1.4.3, the principle of CCM is to predict the current value of the cause variable from the past lags of the consequence variable. A causal relationship from $y$ to $x$ is estimated if the lags of $x$ contain information to predict $y$. We will use a prediction method similar to the simplex projection, but here from one variable $x$ to another $y$.

The principle is to use a similar argument of continuity in the path of the attractor in the embedding space, and the mapping between the embedding space and the initial phase space. If the nonparametric prediction is efficient, time points close together in the embedding space of $x$ should have similar values of $y$. This idea is presented in the Figure 14 for the stock MORWONGESE and $E = 3$: if SST causes productivity, we expect the points close to each other in the embedding space of productivity to have similar values of SST (similar colors on the graph). Note that the optimal embedding dimension determined with the simplex projection was $E = 4$ for the MORWONGESE stock, but is

presented here with $E = 3$ for visualization purposes only (3D plot).

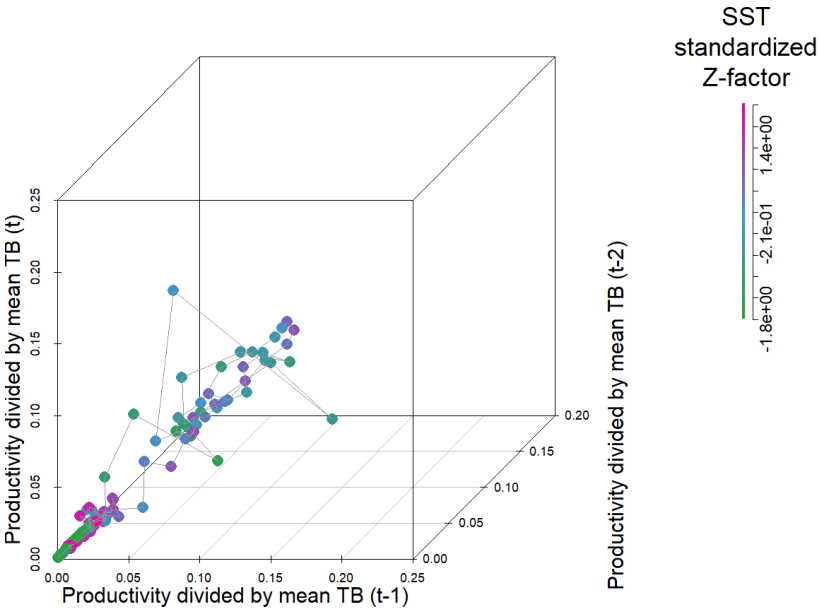


**Figure 14:** Example of embedding space of 3 dimensions of productivity for the stock MORWONGESE. The points are colored by the SST. $E = 3$ is not the optimal $E$ for this stock, but is chosen only to allow a 3D visualization. Points close in the embedding space of productivity should have similar values of SST (color) if SST causes productivity.

Let $E$ be the optimal dimension chosen with the method based on the simplex projection presented in section 2.3. We consider the embedding space containing the vectors $\underline{\boldsymbol{X}}(t) = (x(t-(E-1))\ ,\ x(t-(E-2))\ ,\ \ldots\ ,\ x(t-1)\ ,\ x(t))$, and we want to predict the value of $y$ at some time $t^*$. Here in the CCM, we do not consider all the points $\underline{\boldsymbol{X}}(t)$ in the embedding space, but only $L$ points randomly chosen from all the points in the embedding space (except $\underline{\boldsymbol{X}}(t^*)$). These points are called library points, and $L$ is the library size. Then we select the $E+1$ nearest neighbors of $\underline{\boldsymbol{X}}(t^*)$ in the embedding space, but only among the $L$ library points. Let $\underline{\boldsymbol{X}}(t^j)$ for $j \in \{1, \ldots, E+1\}$ be these $E+1$ nearest neighbors of $\underline{\boldsymbol{X}}(t^*)$ among the library points. We can predict $\hat{y}(t^*)$ depending on the observed values $y(t_j)$ of the nearest neighbors:

$$\hat{y}(t^*) = \sum_{j=1}^{E+1} w_j y(t^j) \quad \text{with } w_j = \frac{u_j}{\sum_{k=1}^{E+1} u_k} \text{ and } u_i = \exp\left\{ -\frac{\left\| \underline{\boldsymbol{X}}(t^i) - \underline{\boldsymbol{X}}(t^*) \right\|}{\left\| \underline{\boldsymbol{X}}(t^1) - \underline{\boldsymbol{X}}(t^*) \right\|} \right\} \tag{9}$$

Again, we compute a forecasting skill $\rho$ for the CCM as the correlation between the observed values of $y$ and the predicted values $\hat{y}$ for all points in the time series. Since

the selection of the $L$ library points is random, we perform 100 bootstraps, each with a random selection of the $L$ points in the library. Then, for each library size, we obtain a distribution of predictions for each time point and the associated forecasting skill for the entire time series for a given library size $L$.

We can run the CCM for different values of the library size $L$ and compute the forecasting skill for each value of $L$. We applied it to 20 different library sizes, evenly distributed between 5 and the maximum library size (time series length minus $E$). The forecasting skill as a function of the library size is shown in the Figure 15 for the productivity of the stock MORWONGESE. Note that when $L$ is low, we do not consider many points, so the nearest neighbors can be quite bad candidates for points close to the point of interest, and we expect the forecasting skill to be low. As $L$ increases, if the causal relationship is strong, the forecasting skill should increase.

This increase in forecasting skill is shown in Figure 15 in the cross-mapping from productivity to SST for the stock MORWONGESE. The predictions are better as the library size increases (median prediction per year in blue solid line and 5-95% quantiles in blue band, among the 100 bootstraps). The comparison of observed and predicted values is presented in Supplementary Materials Figure 31.

The increase in forecasting skill with library size is generally referred to as "*convergence*".

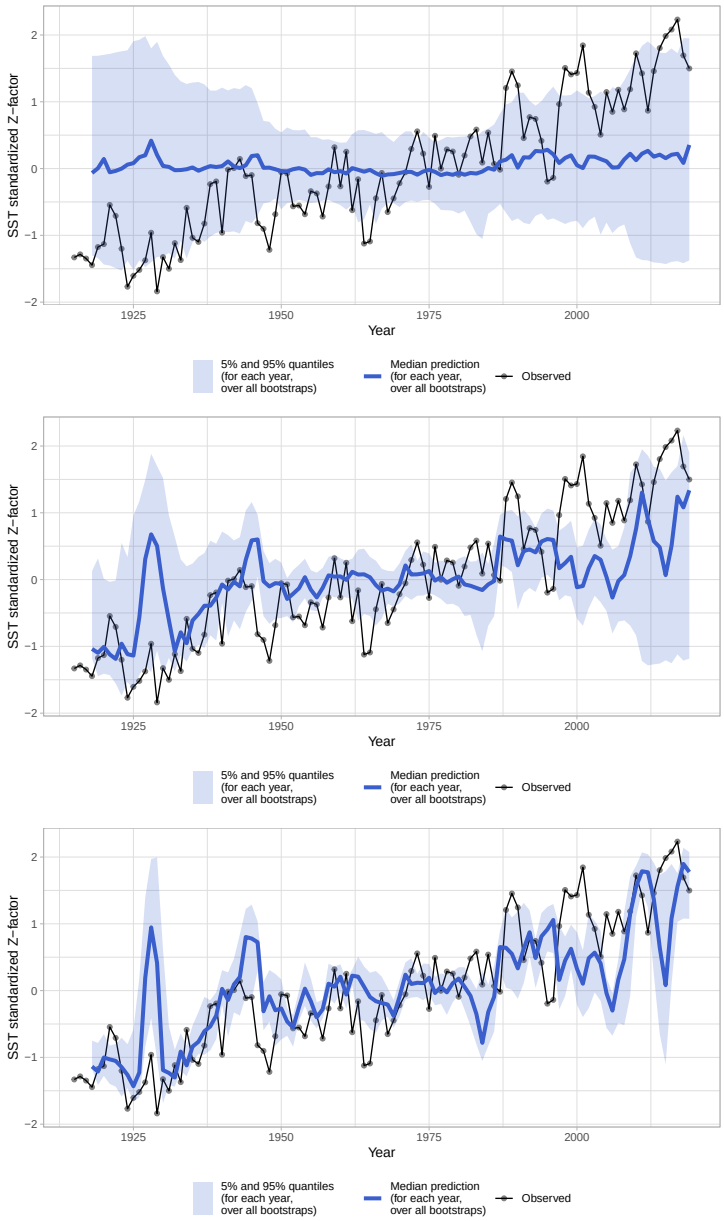


**Figure 15:** Prediction of SST from productivity in the CCM (optimal $E = 4$) for library sizes $L = 5$ (top), $L = 37$ (middle), and $L = 105$ (bottom)

## 2.6 Testing the Significance of Causality

To test whether the prediction in the CCM is really due to the lags and the temporal structure of the time series, we compared the increase in forecasting skill with library size to the behavior of a "*null model*" through surrogate time series (Chang et al., 2017; Koutsodendris et al., 2023). To do this, we randomly shuffled the time indices in the time series of both variables $x$ and $y$ (keeping the correspondence between $x$ and $y$ during the shuffling), and we applied the CCM with the same procedure as before for each random shuffle, but here with only one bootstrap for each shuffle. We ran 100 random shuffles. We

then computed the forecasting skill for each library size and for each random shuffle. We get a distribution of forecasting skills for each library size and for this *null model*, which will be the reference of the time series where we do not expect any *convergence* in the CCM, since we have removed the temporal structure of the time series. The Figure 16 shows the convergence for the CCM from productivity to SST for the stock MORWONGESE, with the forecasting skill of the cross-mapping depending on the library size $L$, for the original time series and the surrogates. An example without convergence in the CCM is presented in the Supplementary Materials Figure 32.

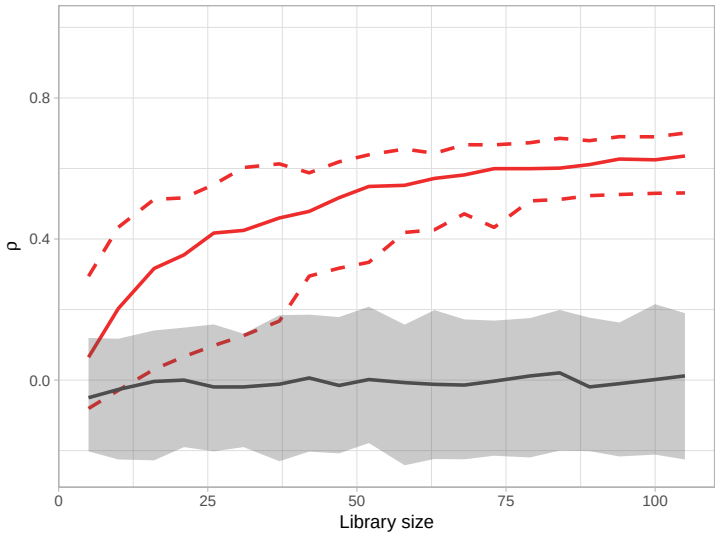


**Figure 16:** Convergence for the CCM from productivity to SST for the MORWONGESE stock, where the forecasting skill of the cross-mapping depends on the library size $L$. The red curves represent the CCM applied to the original data (median of the 100 bootstraps for each $L$ in the solid line, and 5-95% quantiles in the dashed line). The grey curve represents the median of the forecasting skills for the 100 random shuffles (*null model*). The grey ribbon represents the 5-95% quantiles of forecasting skills for the 100 random shuffles.

To assess whether there is causality between the variables, we applied two criteria: the forecasting skill should increase with the library size, and the forecasting skill should be higher than the forecasting skill of the *null model*.

To test whether the forecasting skill increases with library size, we use a Mann-Kendall test. A Mann-Kendall test is a nonparametric test that assesses a monotonous trend based on the ranks of the values (Mann, 1945). This test returns a value $\tau$ that is positive if the forecasting skill increases with library size and negative if the forecasting skill decreases with library size. It also provides a p-value for the significance of the monotonic trend. So we check if $\tau$ is positive and if the p-value is less than 0.05.

To check if the forecasting skill is higher than the forecasting skill of the *null model*

for the same library size, we check if the median forecasting skill of the 100 bootstraps on the original data is above the 95% quantile of the 100 random shuffles for at least 90% of the library sizes.

The two tests are illustrated in the Supplementary Materials Figure 33. In this step, we can assess whether there is a causal relationship from a time series $y$ to a time series $x$.

## 2.7 Confidence and Causal Strength

We can estimate proxies for the confidence we can have in the causality assessment from the previous section. Causality was assessed in the case of a *convergence*, which means a better forecasting skill as we increase the library size. To quantify this convergence, we define several metrics:

- The maximum forecasting skill ($\rho_{\max}$) among all library sizes, at the median of the bootstraps on the original data. This is the maximum value of the red solid curve in the Figure 16 in the example of the stock MORWONGESE. This value reflects how good the prediction can be at best, which gives an idea of how much information is contained in the lags of the time series of the consequence variable to predict the current value of the cause variable.

- The rate of increase in forecasting skill between the smallest and largest library sizes: $\frac{\rho(\text{max library size}) - \rho(\text{min library size})}{\text{max library size} - \text{min library size}}$. This value reflects how much the forecasting skill increases with library size, giving an idea of how much information is added to the prediction when we observe new points in the embedding space.

- Area between the median of the bootstraps on the original data and the median of the shuffles on the null data, divided by the range of the library sizes (to get a value standardized between -1 and 1 for all the stocks): $\frac{\int_{\text{max library size}}^{\text{min library size}} \rho_{\text{original}} - \rho_{\text{null}}}{\text{max library size} - \text{min library size}}$. This is the normalized area between the red and grey solid curves in the Figure 16 in the MORWONGESE stock example. This value reflects how much of the information in the prediction is provided by the temporal structure of the time series rather than the random structure of the time series for each library size.

For these 3 metrics, the higher the metric, the more confidence we can have in the causality (we can refer to Figure 16 to visualize this). We compute the 3 metrics to assess the robustness of the method for quantifying confidence in causality, since we did not find clear arguments for preferring one over the other.

Furthermore, we can assess the strength of causality by quantifying the magnitude of the effect of the cause variable on the consequence variable and the sign of the effect, which is positive or negative, depending on whether the cause variable generally increases or decreases the consequence variable. To do this, we consider a method related to S-map forecasting in the phase space of the observed variables (Ushio et al., 2018; Wang et al., 2020). This method has already been applied to ecological data (Rigal et al., 2023).

Let $\boldsymbol{\eta}(t) = (x(t)\ ,\ y(t)\ ,\ \ldots\ ,\ z(t))$ be the observed state variable (i.e., the vector of all variables observed at a given time $t$, in our case productivity, SST, and harvest rate). This vector space should follow the attractor manifold. Here we consider the effect of $y$ on $x$. We assess the strength of causality by a linear approximation of the dynamics at each time step. More specifically, for each $t^* \in \{t_1\ ,\ \ldots\ ,\ t_n\}$, we approximate $y(t^*+1)$ by a linear regression of all variables at time $t^*$ (recall that in the EDM framework, a causality from $y$ to $x$ is reflected by the information contained in $x$ to predict $y$). The associated prediction $\hat{y}(t^*+1)$ is defined as:

$$\hat{y}(t^*+1) = c^{t^*}_{y,0} + c^{t^*}_{y,x}x(t^*) + c^{t^*}_{y,y}y(t^*) + \ldots + c^{t^*}_{y,z}z(t^*) \tag{10}$$

If we write this linear approximation for each variable, we get:

$$\begin{aligned} \forall t^*\ ,\ \hat{\boldsymbol{\eta}}(t^*+1) &= \begin{pmatrix} c^{t^*}_{x,0} + c^{t^*}_{x,x}x(t^*) + c^{t^*}_{x,y}y(t^*) + \ldots + c^{t^*}_{x,z}z(t^*) \\ c^{t^*}_{y,0} + c^{t^*}_{y,x}x(t^*) + c^{t^*}_{y,y}y(t^*) + \ldots + c^{t^*}_{y,z}z(t^*) \\ \vdots \\ c^{t^*}_{z,0} + c^{t^*}_{z,x}x(t^*) + c^{t^*}_{z,y}y(t^*) + \ldots + c^{t^*}_{z,z}z(t^*) \end{pmatrix} \\ &= C^{t^*}\tilde{\boldsymbol{\eta}}(t^*) \\ \text{with } C^{t^*} &= \begin{pmatrix} c^{t^*}_{x,0} & c^{t^*}_{x,x} & c^{t^*}_{x,y} & \ldots & c^{t^*}_{x,z} \\ c^{t^*}_{y,0} & c^{t^*}_{y,x} & c^{t^*}_{y,y} & \ldots & c^{t^*}_{y,z} \\ \vdots & \vdots & \vdots & \ddots & \vdots \\ c^{t^*}_{z,0} & c^{t^*}_{z,x} & c^{t^*}_{z,y} & \ldots & c^{t^*}_{z,z} \end{pmatrix} \text{ and } \tilde{\boldsymbol{\eta}}(t^*) = \begin{pmatrix} 1 \\ x(t^*) \\ y(t^*) \\ \vdots \\ z(t^*) \end{pmatrix} \end{aligned} \tag{11}$$

Here, we see that $\hat{\boldsymbol{\eta}}(t^*+1) = C^{t^*}\tilde{\boldsymbol{\eta}}(t^*)$ is a linear approximation of a dynamics $\hat{\boldsymbol{\eta}}(t^*+1) = F\,(t^*\ ,\ \tilde{\boldsymbol{\eta}}(t^*))$. The row $y$ of the matrix $C^{t^*}$ gives the coefficients $c^{t^*}_{y,0}\ ,\ c^{t^*}_{y,x}\ ,\ c^{t^*}_{y,y}\ ,\ \ldots\ ,\ c^{t^*}_{y,z}$ of the linear regression, which are the strength of the causal relationship from $y$ to each variable (intercept, $x$, $y$, $\ldots$, $z$) at the time $t^*$.

We have only one realization of the equality Eq. (10) (a single realization of $\hat{y}(t^*+1)$), but to estimate the matrix of coefficients $C^{t^*}$ we need more realizations. So we artificially consider all points in the state space (not just the one at time $t^*$), but with an

exponentially decreasing weight, since the linear approximation only makes sense locally. The exponential decay rate of the weight depends on the optimal parameter $\theta$, which was evaluated with S-map forecasting to estimate the degree of nonlinearity of the dynamics. For the coefficients at the given time $t^*$, we consider all the points $t_k \in \{t_1\,,\,\ldots\,,\,t_n\}$, and Eq. (10) becomes:

$$\begin{aligned}
&\forall k \in \{1,\ldots,n\}\ ,\ w_k^{t^*} y(t_k+1) = c_{y,0}^{t^*} w_k^{t^*} + c_{y,x}^{t^*} x(t_k) w_k^{t^*} + c_{y,y}^{t^*} y(t_k) w_k^{t^*} + \ldots + c_{y,z}^{t^*} z(t_k) w_k^{t^*} + \epsilon_k^{t^*} \\
&\qquad \text{with } w_k^{t^*} = \exp\left\{-\theta \frac{\|\boldsymbol{\eta}(t_k) - \boldsymbol{\eta}(t^*)\|}{\frac{1}{n}\sum_{l=1}^{n} \|\boldsymbol{\eta}(t_l) - \boldsymbol{\eta}(t^*)\|}\right\} \text{ the weight of the point } k \\
&\qquad \text{and where } \theta \text{ is the degree of non-linearity, assessed with the S-map} \\
&\qquad \text{and } \epsilon_k^{t^*} \text{ the residuals, for instance assumed normally distributed}
\end{aligned} \tag{12}$$

Now let us define:

$$\begin{aligned}
B_y &= \begin{pmatrix} w_1^{t^*} y(t_1+1) \\ \vdots \\ w_n^{t^*} y(t_n+1) \end{pmatrix}\ ,\ A_y = \begin{pmatrix} w_1^{t^*} & x(t_1)w_1^{t^*} & y(t_1)w_1^{t^*} & \ldots & z(t_1)w_1^{t^*} \\ \vdots & \vdots & \vdots & \ddots & \vdots \\ w_n^{t^*} & x(t_n)w_n^{t^*} & y(t_n)w_n^{t^*} & \ldots & z(t_n)w_n^{t^*} \end{pmatrix}\ , \\
C_y^{t^*} &= \begin{pmatrix} c_{y,0}^{t^*} \\ c_{y,x}^{t^*} \\ c_{y,y}^{t^*} \\ \vdots \\ c_{y,z}^{t^*} \end{pmatrix} \text{ the vector of row } y \text{ in } C^{t^*}\ ,\ \text{and } \epsilon^{t^*} = \begin{pmatrix} \epsilon_1^{t^*} \\ \vdots \\ \epsilon_n^{t^*} \end{pmatrix} \text{ the residuals}
\end{aligned} \tag{13}$$

We obtain the linear system $B_y = A_y C_y^{t^*} + \epsilon^{t^*}$, and we can estimate the coefficients as in least-squares for a linear regression to get:

$$C_y^{t^*} = (A_y^T A_y)^{-1} A_y^T B_y \tag{14}$$

When we consider the causal relationship from $y$ to $x$, we focus on the coefficient $c_{y,x}^{t^*}$, at time $t^*$. The overall strength of the causal link from $y$ to $x$ is then defined as the average of $c_{y,x}^{t^*}$ over all times $t^* \in \{t_1\,,\,\ldots\,,\,t_n\}$.

All this causality strength estimation is available in the R package `rEDM` with the function `block_lnlp` (including minor changes from the source code to avoid errors).

## 2.8 Ecological Patterns in Causality

We expect different responses of fish stocks to drivers. Therefore, we try to identify ecological patterns in the functional traits that are related to causality. We use the following functional traits from the FishBase and FishLife databases (Froese and Pauly, 2024; Thorson, 2020):

- $L_\infty$ (`Loo` in `R`): mean asymptotic length, i.e. the length they would reach at infinite age (see details here)
- $K$: growth rate, used in the von Bertalanffy growth function formula: $L_t = L_\infty \left(1 - \mathrm{e}^{-K(t-t_0)}\right)$
- $W_\infty$ (`Winfinity` in `R`): average asymptotic weight, i.e. the weight they would reach at infinite age.
- $t_{\max}$ (`tmax` in `R`): maximum age of the fish
- $t_m$ (`tm` in `R`): age at first maturity
- $M$: natural mortality (see details here)
- $L_m$ (`Lm` in `R`): length at first maturity
- Temperature: average environmental temperature
- `FoodTroph`: trophic level of the fish

We also consider the management status and trends associated with the fish stocks, calculated from the RAMLDB:

- `mean_B_prshf`: mean biomass divided by biomass at maximum sustainable yield along the time series
- `sum_C_prshf`: sum of total catches along the time series
- `mean_U_prshf`: mean of `UdivUmsypref` (harvest rate) along the time series
- `U_change_prshf`: coefficient of the slope of `UdivUmsypref` (harvest rate) as a function of years, estimated by linear regression
- `mean_ER_prshf`: mean of the exploration rate along the time series
- `ER_change_prshf`: coefficient of the slope of the exploration rate as a function of years, estimated by linear regression

The values of the functional traits are presented in the Supplementary Materials Figure 34.

We then analyzed the effect of the functional characteristics on the confidence in the estimated causal relationship and the strength of the causality. To do so, for each trait or management status or trend presented above, we applied a linear model of the trait or management status or trend, depending on the confidence in the causality (e.g., $\rho_{\max}$) and the strength of the causality (here, the average along time of $c^{t^*}$ presented in the previous section). We tested the significance of the effect of the trait (or management status or trend) on the confidence (or strength) of the causality, using a threshold of 5% for the p-value in the test of nullity of the slope coefficient in the linear model.

Furthermore, since the values of confidence and strength of causality may be sensitive to definition, we applied these models using the ranks of the values of confidence and strength of causality among all stocks as explanatory variables.

# 3 Results

## 3.1 Assessing Links from Correlation

We computed the Spearman correlation between the variables as shown in Figure 17, aggregating all stocks and for each stock separately.

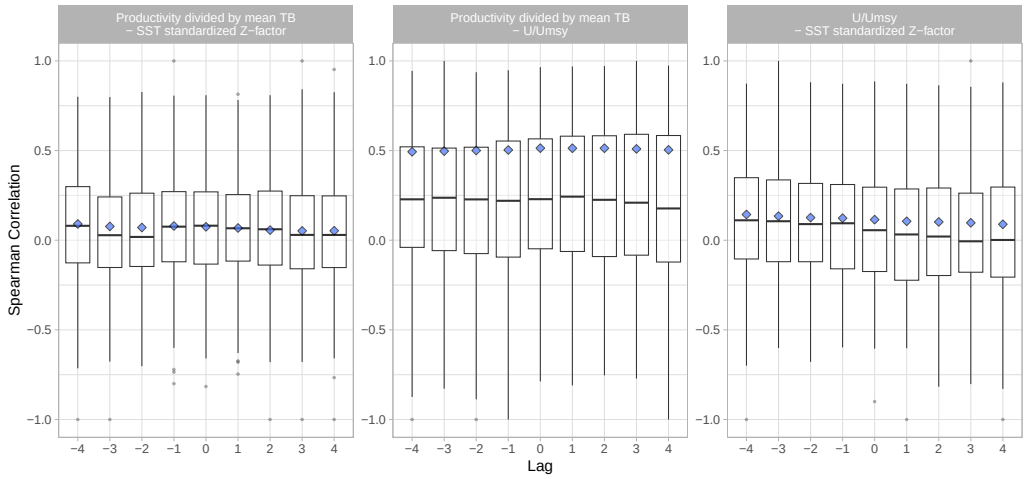


**Figure 17:** Spearman correlation between pairs of variables including lags between -4 and 4 years. The blue squares show the correlation by aggregating all stocks (global correlation) and the box plots show the distribution of correlations for each stock separately (correlation per stock).

We do not find a clear correlation between productivity and SST, as the correlation is low and the boxes overlap with 0, regardless of the lag used between the variables. We observe the same lack of a clear correlation between harvest rate and SST. A positive correlation appears between productivity and harvest rate (squares around a correlation of 0.5 and boxplots almost above 0).

A similar correlation method is presented in the Supplementary Materials Figure 35, Figure 36, and Figure 37, using linear models between the time series $x(t + l)$ and $y(t)$, for each pair of variables and lags $l$ between -4 and 4.

## 3.2 Simplex Projection - Estimating the Embedding Dimension

After the filtering process presented in section 2.3 (more than 40 data points and positive forecasting skill at the optimal embedding dimension), we retained 153 stocks for the productivity embedding study, 151 for the SST, and 154 for the harvest rate.

The optimal embedding dimensions identified for each stock from the process using simplex projection are shown in Figure 18. Most of the optimal embedding dimensions are found below 5.

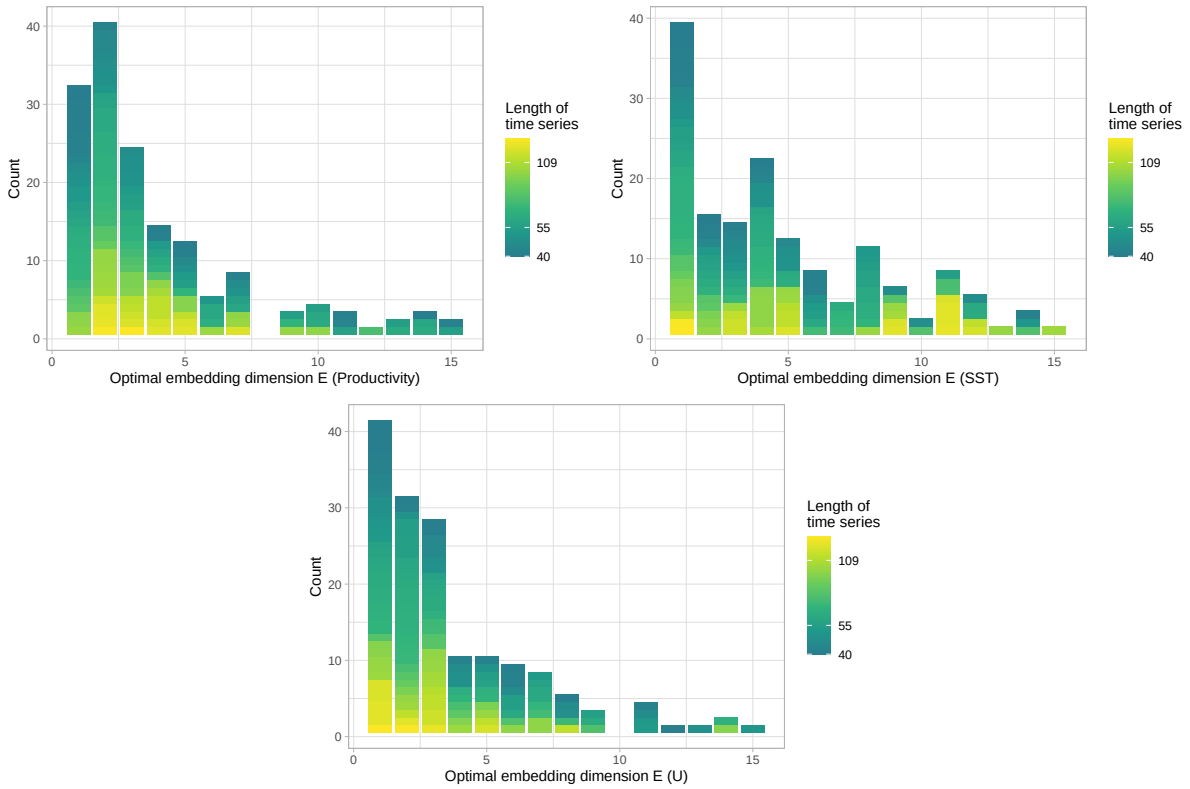


**Figure 18:** Histogram of optimal embedding dimensions $E$, estimated from the simplex projection for each stock, colored by time series length. Top left: productivity, top right: SST, bottom: harvest rate.

We also visually check whether the forecasting skill in the simplex projection decreases with the time horizon (predicting further into the future should be worse if we capture some of the dynamics of the system and not just randomness). For most stocks, the forecasting skill decreases with the time horizon, and the mean forecasting skill of the stocks also decreases with the time horizon, as shown in Figure 19.

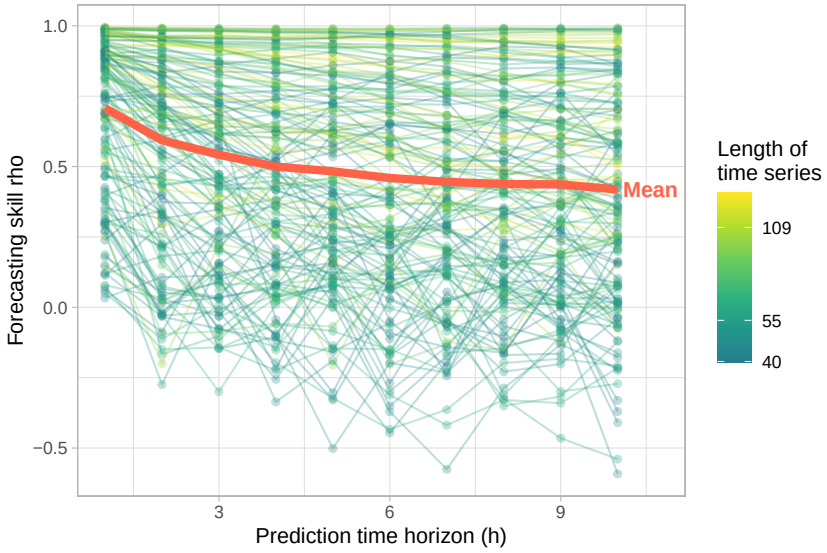


**Figure 19:** Forecasting skill as a function of the time horizon of prediction for all stocks (simplex projection on productivity). The curves are colored according to the length of the time series. The red curve is the mean of the forecasting skill among the stocks, for each time horizon.

## 3.3 S-map - Estimating the nonlinearity

The forecasting skill of the S-map as a function of the nonlinearity parameter $\theta$ is shown in Figure 20 for productivity. In general, we see a maximum of forecasting skill for a particular value of $\theta$ for each stock. This value of $\theta$ informs us of the nonlinearity of the system for the stock in question.

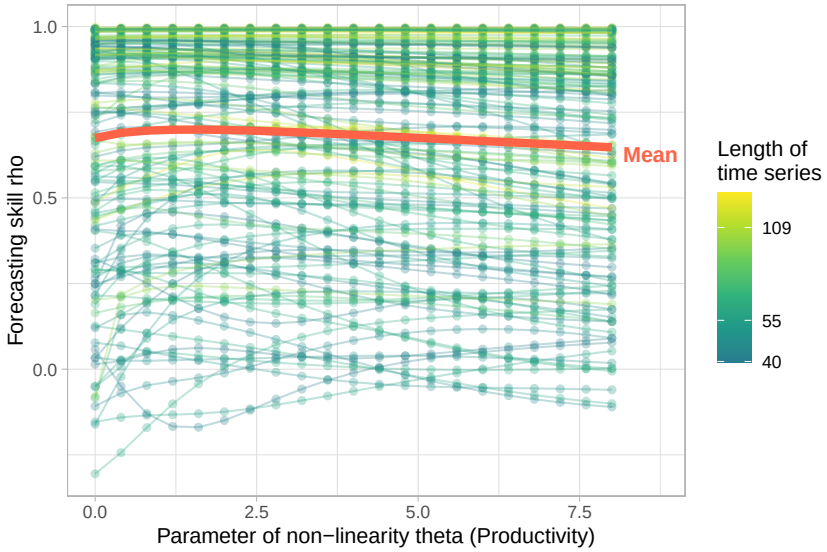


**Figure 20:** Forecasting skill depending on the nonlinearity parameter $\theta$ for all stocks (S-map forecasting on the productivity, using the optimal embedding dimension for the parameter $E$). A higher value of $\theta$ means a higher degree of nonlinearity used for the S-map forecasting. The curves are colored by the time series length. The red curve is the mean of the forecasting skill among the stocks, for each value of $\theta$.

In the S-map forecasting on productivity, the nonlinearity parameter $\theta$ with the highest forecasting skill is strictly between 0 and 8 for about 2/3 of the stocks (Figure 21). This means that we identify nonlinearity for these stocks and quantify a proxy for their degree of nonlinearity. Similar results are found for SST and harvest rate as shown in Figure 21.

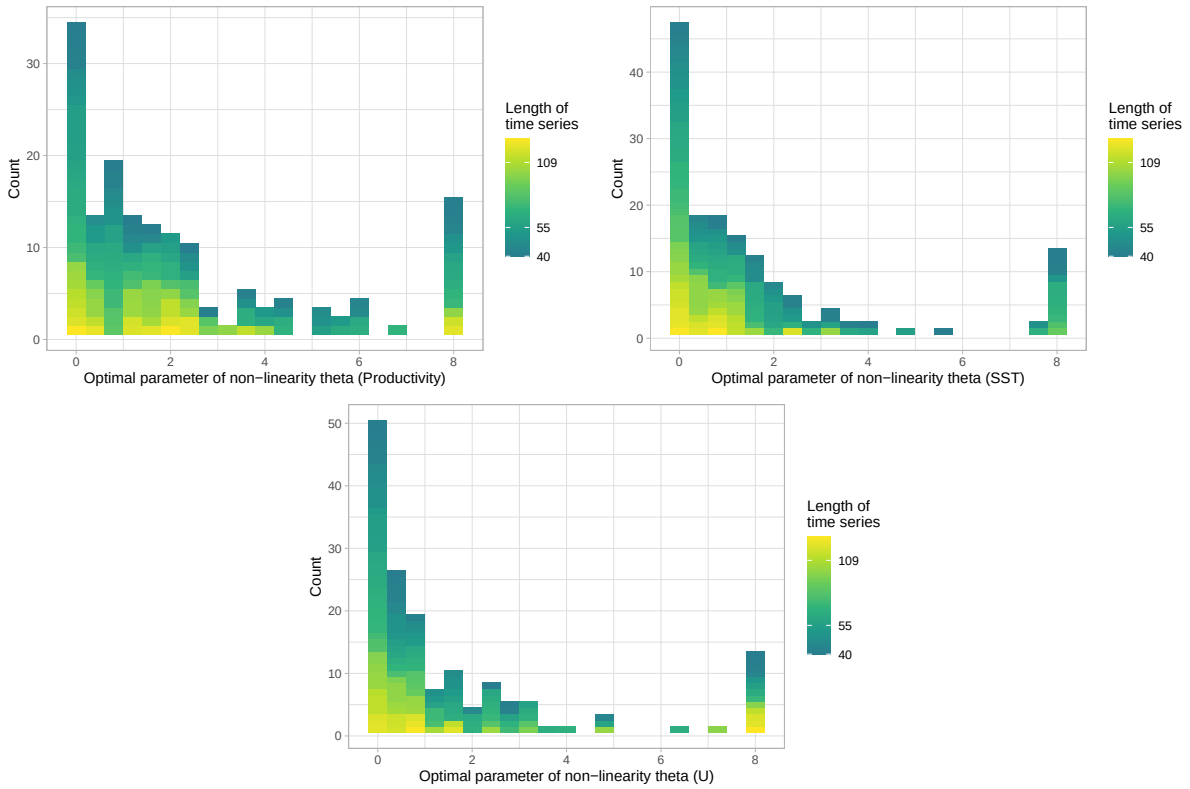


**Figure 21:** Histograms of the optimal nonlinearity parameters $\theta$ (with the highest forecasting skill) using the optimal embedding dimension defined by the simplex projection. Top left: productivity, top right: SST, bottom: harvest rate.

## 3.4 Convergent Cross Mapping (CCM) - Inferring and Characterizing Causality

Convergent Cross Mapping (CCM) allows us to detect the causality between the variables. The filtering process presented in the section 2.3 allows us to keep the causality analysis for the stocks with the library variable passing the filtering process - since the embedding is used on the library variable, i.e. the tested consequence variable. The Figure 22 shows the causality assessment for the filtered stocks, for each pair of variables. Remember that $x$ cross-mapped to $y$ assesses whether $y$ causes $x$. We find the highest number of causal relationships from the harvest rate to the productivity (56 stocks) and from the productivity to the harvest rate (45 stocks). 27 stocks show causality from SST to productivity.

Note that we still find causalities from productivity to SST (14 stocks) and from harvest rate to SST (26 stocks).

The details of the causality assessment are presented in the Supplementary Materials Figure 38 for each stock, for productivity cross-mapped to SST.

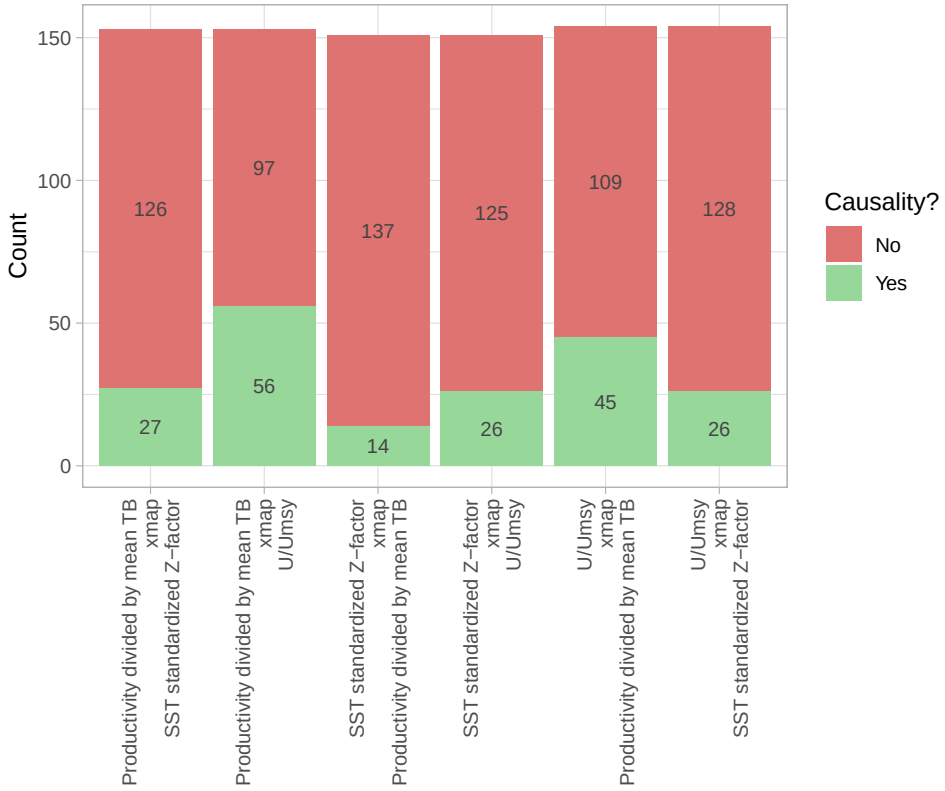


**Figure 22:** Causality detection from tests (Mann-Kendall test and original data over null model) on the CCM for each pair of variables. $x$ cross-mapped to $y$ (written "xmap") assesses whether $y$ causes $x$. Causality is assessed only on the filtered stock (153 stocks when productivity is the library variable, 151 for SST, and 154 for harvest rate)

The three metrics of confidence in causality and metric of strength of causality are shown for each stock and each pair of variables in Figure 23. These pair plots show the relationships between the metrics. The correlations between the metrics are not very clear, except between the rate of increase in forecasting skill and the Area Under the Curve in the CCM.

If we look at the ranks of the values of the metrics among the pairs of variables (ranking all stocks evaluated), we find similar results (Figure 23 in the graph below). We find negative correlations between the causality confidence rank and the causality strength rank.

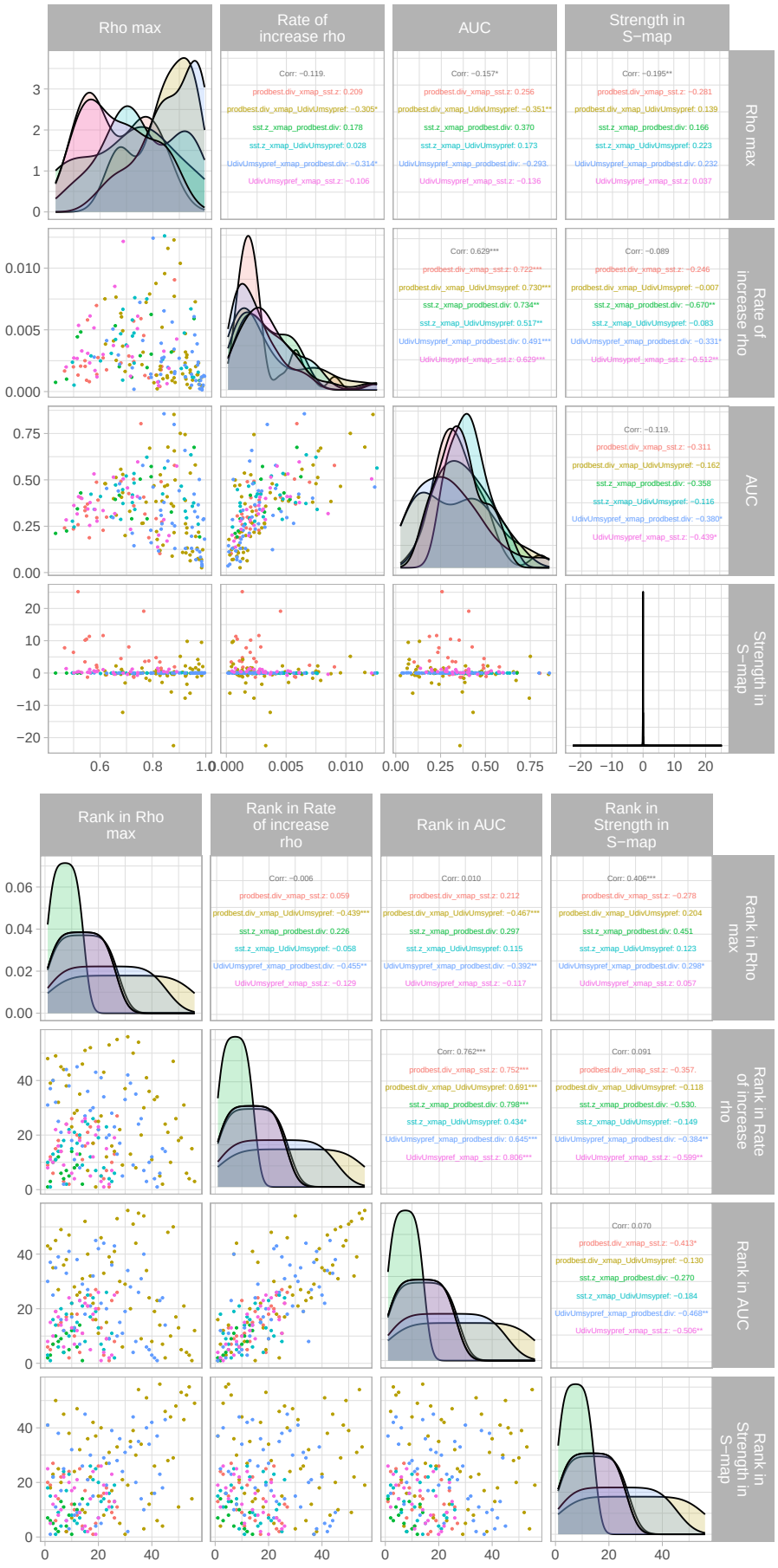


**Figure 23:** Pair plot of metrics of confidence in causality and strength of causality. Colors represent the pair of variables tested for causality. Top: Values of the metrics. Bottom: Ranks of the metric values.

The strength of causality is shown in the Figure 24. The causal effect of SST on productivity is estimated to be positive for the vast majority of stocks, with larger values than other causal relationships. The effect of harvest rate on productivity is either positive or negative, depending on the stock, and of moderate magnitude. The effect of SST on the harvest rate is generally positive and of small magnitude. In comparison, the causal relationship from productivity or harvest rate to SST is negligible, as is the relationship from productivity to harvest rate.

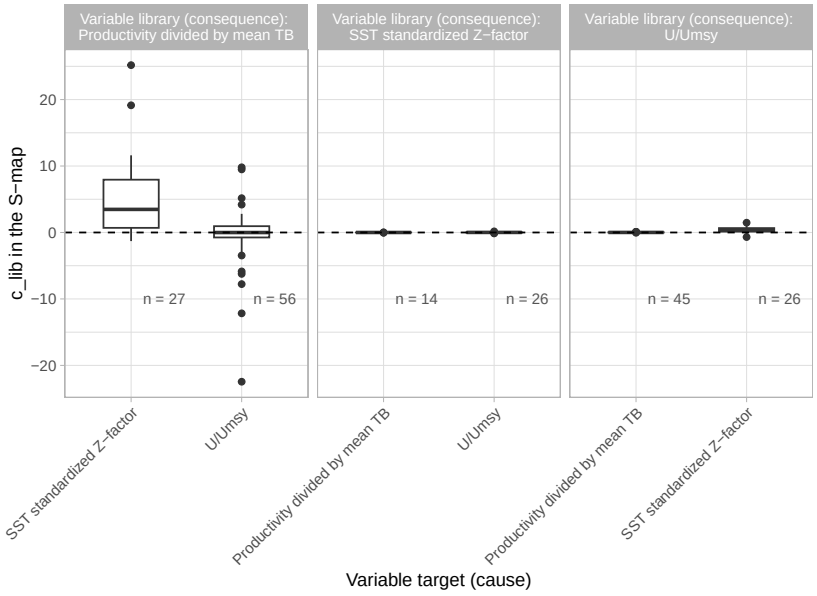


**Figure 24:** Boxplot of the strength of causality using the S-map-related method, for each pair of variables (causal variable on the horizontal axis and consequence variable per panel). Each boxplot contains the strength for the stocks for which we find a causal relationship. `n` is the number of causal relationships identified in Figure 22. `c_lib in the S-map` refers to the mean of $c^{t^*}$ over time for each stock as presented in Section 2.7.

## 3.5 Ecological Patterns in Causality

The linear models of maximum forecasting skill in the CCM, testing the causality from SST to productivity, as a function of functional traits or management status and trends, are shown in Figure 25. Some linear models show a significant effect of the trait on the confidence in the causality. Considering this metric $\rho_{\max}$, higher confidence is associated with higher growth rate ($K$), asymptotic length ($L_\infty$), asymptotic weight ($W_\infty$), natural mortality ($M$), temperature, and total catch (`sum_C_prshf`). Higher confidence is associated with lower age at maturity ($t_m$) and maximum age ($t_{\max}$).

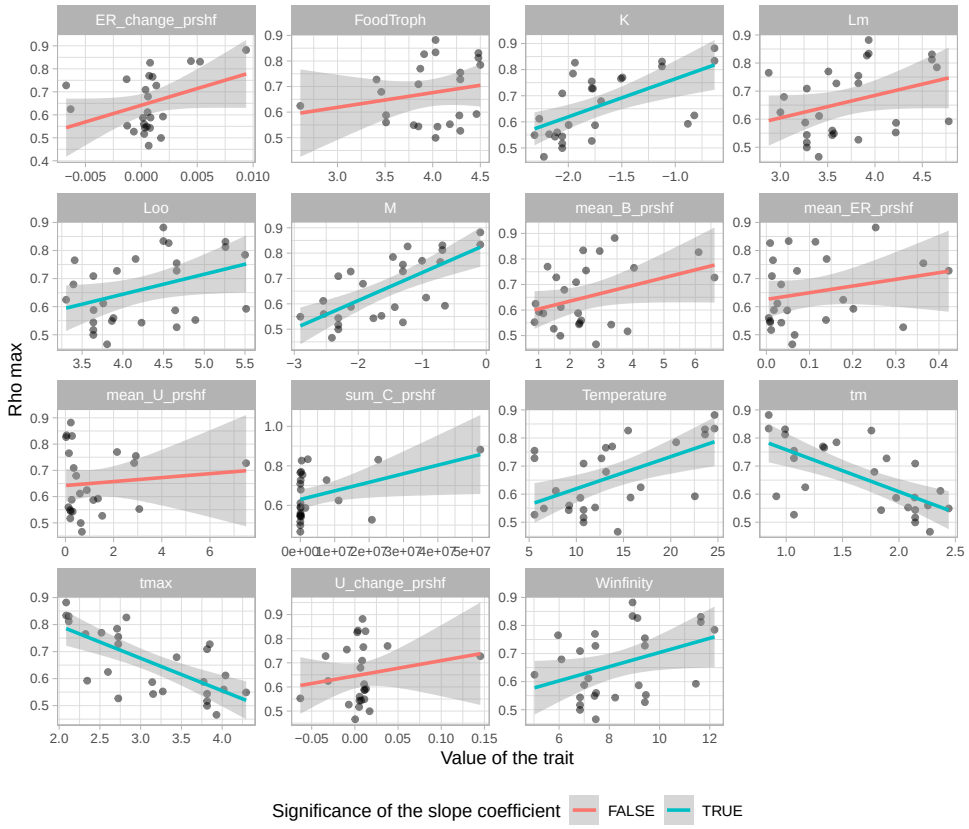


**Figure 25:** Relationships between traits and confidence in causality. Linear models applied to the maximum forecasting skill in the CCM testing the causality from SST to productivity ($\rho_{\max}$) as a function of functional traits or management status and trends. The colors represent the significance in the test of nullity of the slope.

The linear models of the strength of causality in the S-map-related process for the causal link from SST to productivity, as a function of functional traits or management status and trends, are shown in Figure 26. Considering this metric for the strength of causality, greater positive strength is associated with greater age at maturity ($t_m$) and maximum age ($t_{\max}$). A more negative (or smaller) effect is associated with greater asymptotic length ($L_\infty$), length at maturity ($L_m$), asymptotic weight ($W_\infty$), and natural mortality ($M$), mean exploitation rate (`mean_ER_prshf`), and mean harvest rate (`mean_U_prshf`).

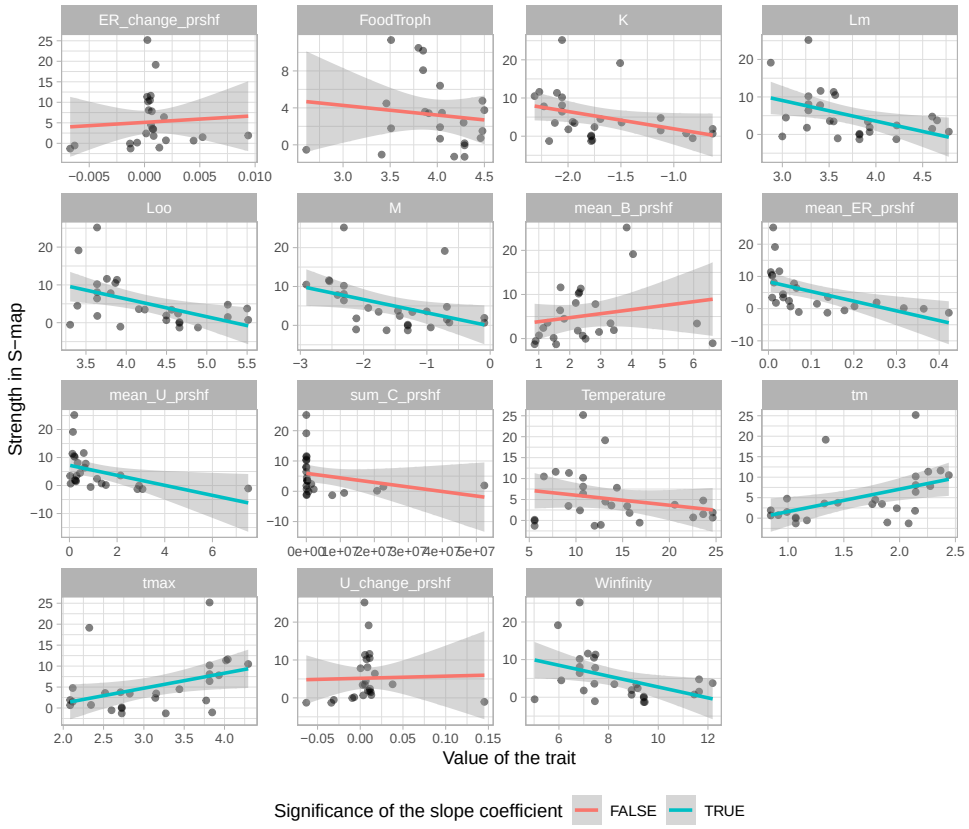


**Figure 26:** Relationships between traits and strength of causality in S-map. Linear models applied to the strength of causality from SST to productivity (mean of $c^{t^*}$ over time) as a function of functional traits or management status and trends. The colors represent the significance in the test of nullity of the slope.

The summary of the significance and sign of the effects of traits and management status and trends on the confidence or strength of causality is presented in the Supplementary Materials Figure 39 for the three causal relationships with non-negligible strength identified in the Figure 24: SST causing productivity, harvest rate causing productivity, and SST causing harvest rate.

# 4 Discussion

## 4.1 Correlations between Time Series

The correlation analysis showed no clear relationship between SST and productivity and between SST and harvest rate. It is not surprising to see no global correlation between productivity and SST, as a relationship between these variables may be more subtle. We did not expect a relationship between SST and harvest rate, as the relationship, if it exists, may be indirect.

We find a positive relationship between productivity and harvest rate. This is consistent with the general pattern of exploited fish stocks. We can explain this with a simple Verhulst logistic growth model: $\frac{dB}{dt} = rB\left(1 - \frac{B}{K}\right)$, where $B$ is the biomass, $r$ is the intrinsic growth rate, and $K$ is the carrying capacity. The Maximum Sustainable Yield is reached at the maximum of the growth rate $rB\left(1 - \frac{B}{K}\right)$, which is at $B_{MSY} = K/2$. Thus, when we start fishing a stock, we decrease the biomass (from $K$ and targeting $B_{MSY} = K/2$) and the growth rate increases (from almost 0 to $rB_{MSY}/2$), which implies an increase in productivity. In this simple example, we see that the general trend is to increase the harvest rate while increasing productivity (and decreasing biomass). This leads to the positive correlation between productivity and harvest rate.

## 4.2 Causality Assessment

In the process of causality assessment using EDM, we identified optimal embedding dimensions for each library variable and for each stock. The dimensions were around 5, which seems to be a consistent range for the dimensionality of the system. We do not expect too high dimensions, as we may assume an underlying dynamic that relates fish stocks to environmental conditions.

The forecasting skill of the simplex projection generally decreases, which is consistent with expectations: if the dynamics follow an underlying dynamic and are not just noise, we expect worse predictions from the simplex projection while predicting further into the future. This supports the use of the EDM method to assess causality.

S-map forecasting identified nonlinearities in some of the stock dynamics ($\theta > 0$). The nonlinearity supports the relevance of EDM methods compared to other methods such as Granger Causality (Sugihara et al., 2012).

The causality assessment identified the highest number of correlations between productivity and harvest rate, in both directions. This is consistent with the literature: fishing pressure (especially overfishing) is the main driver of marine biodiversity (IPBES,

2019). The strength of the causality is either positive or negative depending on the stock. Furthermore, as shown in the Supplementary Materials Figure 39 (middle plot, column "Strength in S-map"), an increasing global trend in harvest rate (`U_change_prshf`) or a high mean harvest rate over time (`mean_U_prshf`) is associated with a more negative effect of harvest rate on productivity. This is consistent with the idea that for overfished stocks (e.g., high and/or globally increasing fishing pressure), productivity decreases when the harvest rate temporarily increases, i.e. overfished stocks are more sensitive to fishing pressure.

We may also observe a feedback loop from productivity to harvest rate, possibly related to adaptive management or incentives for fisheries to increase fishing when stock productivity increases. However, this causal relationship from productivity to harvest rate is associated with negligible strength. Thus, even if a causal relationship from productivity to harvest rate is identified, the effect on average is negligible for all stocks.

Causality from SST to productivity is identified for 27 stocks. This causality is positive: when SST temporarily increases, productivity generally increases. This is not directly consistent with the literature where climate change has negative impacts on marine ecosystems. Here we focus on productivity rather than biomass or abundance. Thus, it may be possible to have an increase in productivity with a decrease in biomass. Furthermore, a poleward shift in distributions may lead to an increase in productivity in some regions. However, it is surprising to observe a positive effect of SST on productivity for almost all stocks in our analysis. A closer look at physiological and ecological mechanisms may help to evaluate this finding. Finally, we must keep in mind that the EDM framework provides causality based on temporally local information (lags until $t - E$). Furthermore, the strength of causality is assessed based on an average along the entire time series of the coefficients of linearization of the dynamics. Thus, causality can be difficult to assess because climate change involves long processes and the effect may change during the time periods.

Extensions of the CCM can estimate the order of magnitude of the time delay in a causal relationship (Ye et al., 2015). This can help to understand the impact of climate change on the productivity of fish stocks, in future work.

Some causal relationships identified with the CCM do not make physical sense: we do not expect a direct effect from productivity to SST and from harvest rate to SST. Causality was estimated from productivity to SST for 14 stocks and from harvest rate to SST for 26 stocks. However, the strength of the causality is negligible in these cases,

meaning that the causality does not have a relevant strength along the time series. It's consistent with our expectations to ignore these causal relationships.

Finally, there is a small positive causal effect from SST to harvest rate. Even though no direct effect is expected, it is possible that there are indirect effects that lead to our assessment of causality.

## 4.3 Ecological Patterns in Causality

We find greater confidence in the causality from SST to productivity ($\rho_{\max}$) for species with higher growth rates, lower age at maturity, or lower maximum age. This is consistent with previous findings that fishes with faster life histories (e.g., faster growth, earlier age at maturity, and shorter life spans) are more responsive to climate change (Free et al., 2019). Fish associated with warmer temperatures provide greater confidence in causality. It is also consistent with the literature where tropical fish are more sensitive and more at risk (Boyce et al., 2022).

The results are consistent for the strength of causality: the effect is less positive for species with lower age at maturity or lower maximum age. We also find that stocks with higher fishing pressure (`mean_U_prshf` and `mean_ER_prshf`) are associated with a more negative effect of SST on productivity, as reported in the literature, where overfished stocks show increased vulnerability and reduced resilience to climate change impacts (Boyce et al., 2022; Cooley et al., 2023; Free et al., 2019).

We find no clear effect of functional traits on the strength of causality from harvest rate to productivity.

## 4.4 Limitations

The EDM methods rely on approximating a manifold based on observed values of a variable. The more data points we have, the more information we get from this approximation. We tested whether the length of the time series had an effect on the process of assessing causality. We use a linear regression to explain the optimal forecasting skill and the optimal embedding dimension in the simplex projection as a function of the length of the time series (Figure 27). The effect of length is significant for the optimal forecasting skill. This is not surprising since the more data we have, the more accurate the prediction can be. However, there is no significant effect of the length of the time series on the optimal embedding dimension. This supports the robustness of the choice of the optimal embedding dimension for causality assessment.

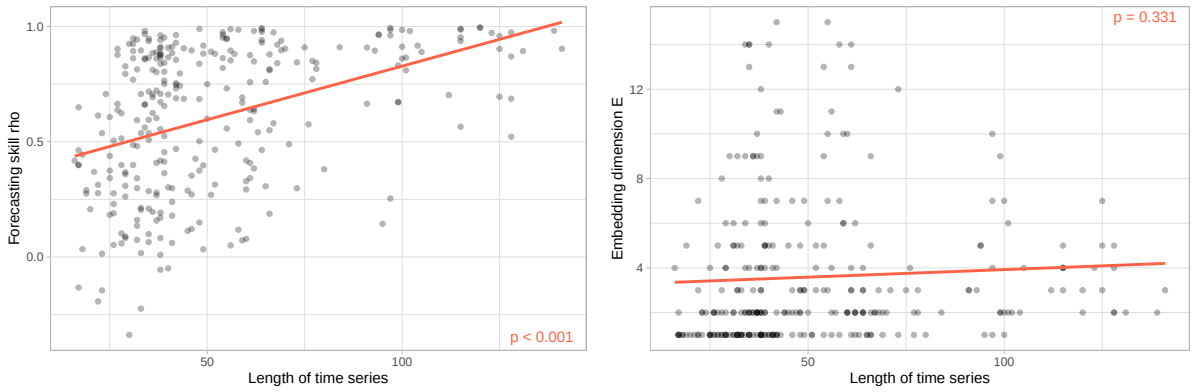


**Figure 27:** Effect of time series length on forecasting skill at the optimal embedding dimension (left) and at the optimal embedding dimension (right) in the simplex projection for all stocks and all variables. The red lines represent the linear regressions with their p-value.

We also applied an ANOVA model to test whether the length of the time series depends on the assessment of causality (Figure 28). The effect is significant in assessing the causality from SST to productivity and from harvest rate to productivity, with longer time series found where causality is identified. These two causal relationships are the most expected in the attribution of drivers of fish stocks. Therefore, we may need longer time series to better study these relationships. With longer time series, we may have identified more causality from SST to productivity and from harvest rate to productivity.

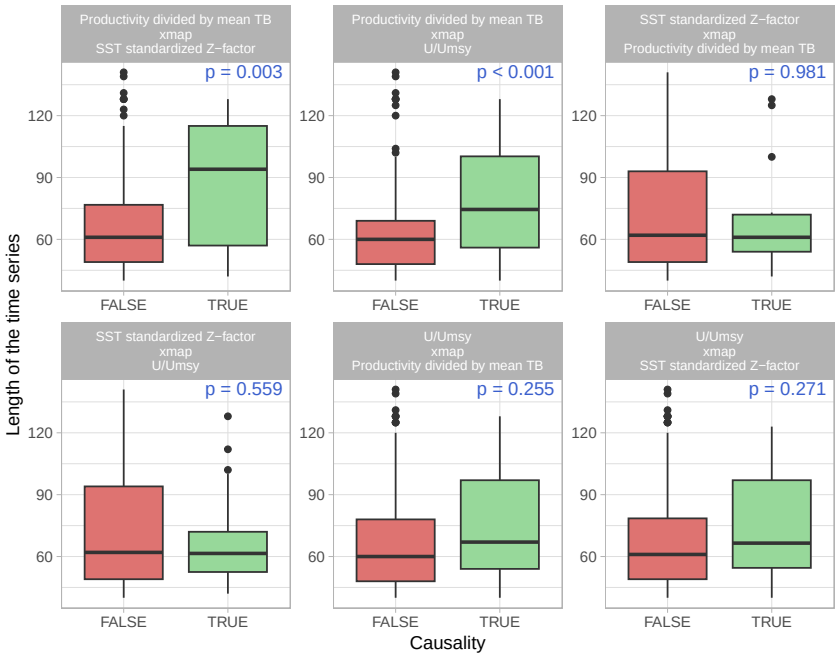


**Figure 28:** Differences in time series length depending on causality assessment, for each pair of variables tested. P-values are from the ANOVA test.

We also tested the effect of time series length on the metrics of confidence and strength in causality in Supplementary Materials Figure 40 and Figure 41. The main patterns are a lower confidence in causality associated with longer time series, and no clear effect of time series length on the strength of causality - suggesting no bias in strength due to time series length.

# 5 Conclusion

## 5.1 Variables of Interest

In this report, we have used SST as a climate variable. However, other variables could also be considered. For example, pH, oxygen content in water, primary productivity, or influxes of particulate organic carbon (POC) are known to affect marine biodiversity (Cooley et al., 2023; Free et al., 2019). In addition, we can examine more variables related to SST than just the annual mean SST, such as maximum temperature, variability, temperature range, etc. Other temperature-related variables may provide better information on the impact of climate change on marine biodiversity, especially for short-term effects.

The approach used in this report can be applied to other time series, which will be the focus of future work.

The same observation can be made for productivity. For example, we can look at the biomass or recruitment of fish stocks. And other variables for fishing pressure can be used, such as exploitation rate, fishing mortality, etc.

## 5.2 Comparison of methods

Other methods to assess the relationship between variables can be explored. Even though Granger Causality is considered to be limited in the case of nonlinear dynamics (Sugihara et al., 2012), Barraquand et al., 2021 found similar results with CCM and Granger Causality in the case of an interaction network and reported no relationship between the degree of nonlinearity of the dynamics and which method performs best between CCM and Granger Causality. Since the EDM methods presented here rely on numerous steps, using a simpler framework may be easier to justify and interpret, especially if the results are similar. Future work may focus on comparing the results of CCM with other methods, such as Granger Causality or other statistical methods on time series.

# References

Barraquand, F., Picoche, C., Detto, M., & Hartig, F. (2021). Inferring species interactions using granger causality and convergent cross mapping. *Theoretical Ecology*, *14*(1), 87–105.

Bellard, C., Marino, C., & Courchamp, F. (2022). Ranking threats to biodiversity and why it doesn't matter. *Nature Communications*, *13*(1), 1–4.

Boyce, D. G., Tittensor, D. P., Garilao, C., Henson, S., Kaschner, K., Kesner-Reyes, K., Pigot, A., Reyes Jr, R. B., Reygondeau, G., Schleit, K. E., et al. (2022). A climate risk index for marine life. *Nature Climate Change*, *12*(9), 854–862.

Chang, C.-W., Ushio, M., & Hsieh, C.-h. (2017). Empirical dynamic modeling for beginners. *Ecological research*, *32*, 785–796.

Cheung, W. W., Watson, R., & Pauly, D. (2013). Signature of ocean warming in global fisheries catch. *Nature*, *497*(7449), 365–368.

Cooley, S., Schoeman, D., Bopp, L., Boyd, P., Donner, S., Kiessling, W., Martinetto, P., Ojea, E., Racault, M., Rost, B., et al. (2023). *Oceans and coastal ecosystems and their services*. https://doi.org/10.1017/9781009325844.005

Dablander, F., et al. (2023). *Changing systems: Statistical, causal, and dynamical perspectives.*

de Carvalho-Souza, G. F., Torres, M. Á., Farias, C., Acosta, J. J., Tornero, J., Sobrino, I., Ramos, F., & Llope, M. (2021). International politics must be considered together with climate and fisheries regulation as a driver of marine ecosystems. *Global Environmental Change*, *69*, 102288.

Deyle, E. R., & Sugihara, G. (2011). Generalized theorems for nonlinear state space reconstruction. *Plos one*, *6*(3), e18295.

Essington, T. E., Moriarty, P. E., Froehlich, H. E., Hodgson, E. E., Koehn, L. E., Oken, K. L., Siple, M. C., & Stawitz, C. C. (2015). Fishing amplifies forage fish population collapses. *Proceedings of the National Academy of Sciences*, *112*(21), 6648–6652.

Free, C. M., Thorson, J. T., Pinsky, M. L., Oken, K. L., Wiedenmann, J., & Jensen, O. P. (2019). Impacts of historical warming on marine fisheries production. *Science*, *363*(6430), 979–983.

Froese, R., & Pauly, D. (2024). Fishbase (R. Froese & D. Pauly, Eds.) [World Wide Web electronic publication]. Retrieved February 2024, from http://www.fishbase.org

Granger, C. W. (1969). Investigating causal relations by econometric models and cross-spectral methods. *Econometrica: journal of the Econometric Society*, 424–438.

Griffith, G. P. (2020). Closing the gap between causality, prediction, emergence, and applied marine management. *ICES Journal of Marine Science*, *77*(4), 1456–1462.

Hilborn, R. (2001). Calculation of biomass trend, exploitation rate, and surplus production from survey and catch data. *Canadian Journal of Fisheries and Aquatic Sciences*, *58*(3), 579–584.

IPBES. (2019, May). *Global assessment report of the intergovernmental science-policy platform on biodiversity and ecosystem services* (E. Brondizio, J. Settele, S. Díaz, & H. T. Ngo, Eds.). https://doi.org/10.5281/zenodo.3831673

Jones, M. C., & Cheung, W. W. (2015). Multi-model ensemble projections of climate change effects on global marine biodiversity. *ICES Journal of Marine Science*, *72*(3), 741–752.

Jones, M. C., & Cheung, W. W. (2018). Using fuzzy logic to determine the vulnerability of marine species to climate change. *Global change biology*, *24*(2), e719–e731.

Koutsodendris, A., Dakos, V., Fletcher, W., Knipping, M., Kotthoff, U., Milner, A., Müller, U., Kaboth-Bahr, S., Kern, O., Kolb, L., et al. (2023). Atmospheric co2 forcing on mediterranean biomes during the past 500 kyrs. nat. commun. 14, 1664.

Mac Nally, R., Thomson, J. R., Kimmerer, W. J., Feyrer, F., Newman, K. B., Sih, A., Bennett, W. A., Brown, L., Fleishman, E., Culberson, S. D., et al. (2010). Analysis of pelagic species decline in the upper san francisco estuary using multivariate autoregressive modeling (mar). *Ecological Applications*, *20*(5), 1417–1430.

Mann, H. B. (1945). Nonparametric tests against trend. *Econometrica: Journal of the econometric society*, 245–259.

Mcowen, C. J., Cheung, W. W., Rykaczewski, R. R., Watson, R. A., & Wood, L. J. (2015). Is fisheries production within l arge m arine e cosystems determined by bottom-up or top-down forcing? *Fish and Fisheries*, *16*(4), 623–632.

Messerli, F. H. (2012). Chocolate consumption, cognitive function, and nobel laureates. *N Engl J Med*, *367*(16), 1562–1564.

Munch, S. B., Rogers, T. L., & Sugihara, G. (2023). Recent developments in empirical dynamic modelling. *Methods in Ecology and Evolution*, *14*(3), 732–745.

Nations, F. (2022). *The state of world fisheries and aquaculture 2022: Towards blue transformation*. FAO. https://books.google.it/books?id=9yN_EAAAQBAJ

Pélissié, M., Devictor, V., & Dakos, V. (2024). A systematic approach for detecting abrupt shifts in ecological timeseries. *Biological Conservation*, *290*, 110429.

Pierre, M., Rouyer, T., Bonhommeau, S., & Fromentin, J.-M. (2018). Assessing causal links in fish stock–recruitment relationships. *ICES Journal of Marine Science*, *75*(3), 903–911.

Prinz, A. L. (2020). Chocolate consumption and noble laureates. *Social Sciences & Humanities Open*, *2*(1), 100082.

Rayner, N., Parker, D. E., Horton, E., Folland, C. K., Alexander, L. V., Rowell, D., Kent, E. C., & Kaplan, A. (2003). Global analyses of sea surface temperature, sea ice, and night marine air temperature since the late nineteenth century. *Journal of Geophysical Research: Atmospheres*, *108*(D14).

Ricard, D., Minto, C., Jensen, O. P., & Baum, J. K. (2012). Examining the knowledge base and status of commercially exploited marine species with the ram legacy stock assessment database. *Fish and fisheries*, *13*(4), 380–398.

Rigal, S., Dakos, V., Alonso, H., Auniņš, A., Benkő, Z., Brotons, L., Chodkiewicz, T., Chylarecki, P., De Carli, E., Del Moral, J. C., et al. (2023). Farmland practices are driving bird population decline across europe. *Proceedings of the National Academy of Sciences*, *120*(21), e2216573120.

Sarkodie, S. A., & Owusu, P. A. (2023). Assessment of global fish footprint reveals growing challenges for sustainable production and consumption. *Marine Pollution Bulletin*, *194*, 115369.

Sharp, G. (1987). Climate and fisheries: Cause and effect or managing the long and short of it all. *South African Journal of Marine Science*, *5*(1), 811–838.

Sugihara, G., May, R., Ye, H., Hsieh, C.-h., Deyle, E., Fogarty, M., & Munch, S. (2012). Detecting causality in complex ecosystems. *Science*, *338*(6106), 496–500. https://doi.org/10.1126/science.1227079

Takens, F. (2006). Detecting strange attractors in turbulence. *Dynamical Systems and Turbulence, Warwick 1980: proceedings of a symposium held at the University of Warwick 1979/80*, 366–381.

Thorson, J. T. (2020). Predicting recruitment density dependence and intrinsic growth rate for all fishes worldwide using a data-integrated life-history model. *Fish and Fisheries*, *21*(2), 237–251.

Thorson, J. T., Cheng, W., Hermann, A. J., Ianelli, J. N., Litzow, M. A., O'Leary, C. A., & Thompson, G. G. (2020). Empirical orthogonal function regression: Linking population biology to spatial varying environmental conditions using climate projections. *Global Change Biology*, *26*(8), 4638–4649.

United Nations, G. A. (2015, October). Transforming our world: The 2030 agenda for sustainable development [United Nations General Assembly Resolution A/RES/70/1, adopted on 25 September 2015, accessed on 15 August 2024]. *United Nations*. https://undocs.org/en/A/RES/70/1

Ushio, M., Hsieh, C.-h., Masuda, R., Deyle, E. R., Ye, H., Chang, C.-W., Sugihara, G., & Kondoh, M. (2018). Fluctuating interaction network and time-varying stability of a natural fish community. *Nature*, *554*(7692), 360–363.

Vert-Pre, K. A., Amoroso, R. O., Jensen, O. P., & Hilborn, R. (2013). Frequency and intensity of productivity regime shifts in marine fish stocks. *Proceedings of the National Academy of Sciences*, *110*(5), 1779–1784.

Wang, J., Kuo, T., & Hsieh, C. (2020). Causal effects of population dynamics and environmental changes on spatial variability of marine fishes. nat commun 11, 2635.

Ye, H., Deyle, E. R., Gilarranz, L. J., & Sugihara, G. (2015). Distinguishing time-delayed causal interactions using convergent cross mapping. *Scientific reports*, *5*(1), 14750.

# Supplementary material

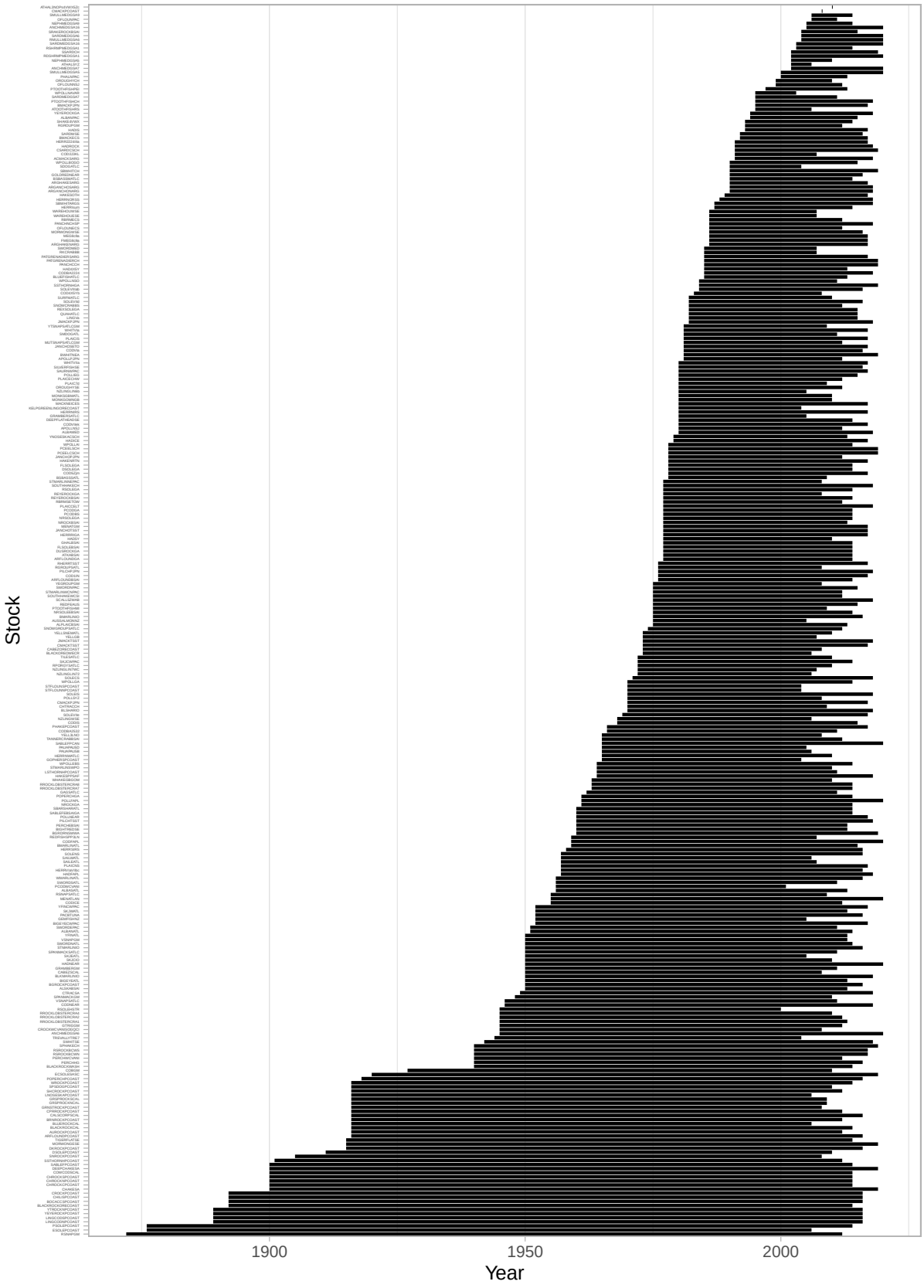


**Figure 29:** Duration of the time series for each stock used from RAMLDB

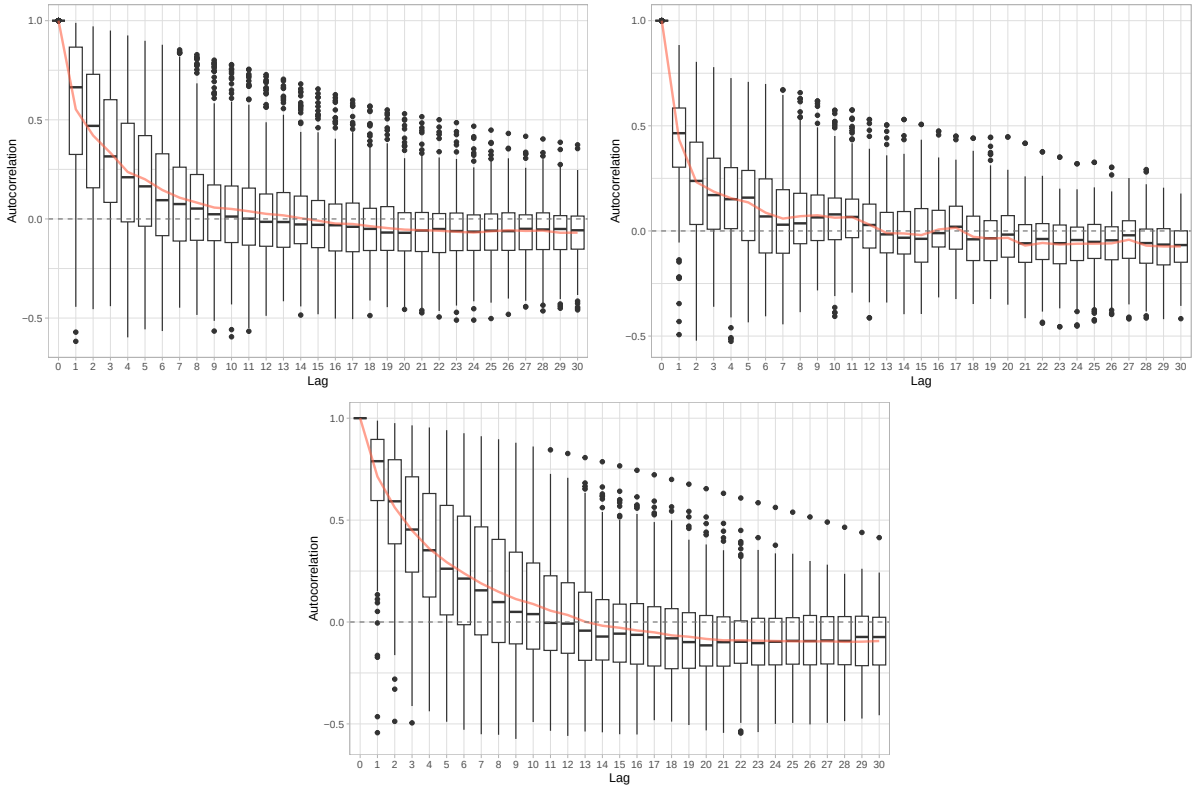


**Figure 30:** Autocorrelations within the time series of productivity, SST and harvest rate. The red curve represents the mean autocorrelation for each lag. The boxplots represent the autocorrelation for each stock.

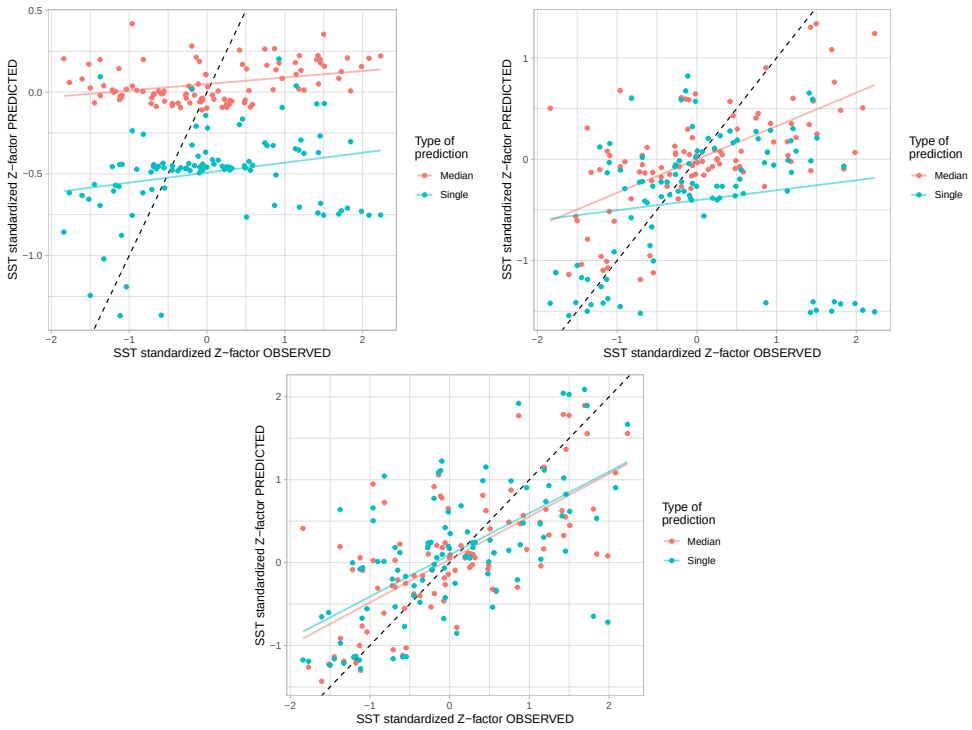


**Figure 31:** CCM prediction vs observed for the stock MORWONGESE in productivity cross-mapped with temperature with the libsize of 5, 37 and 105

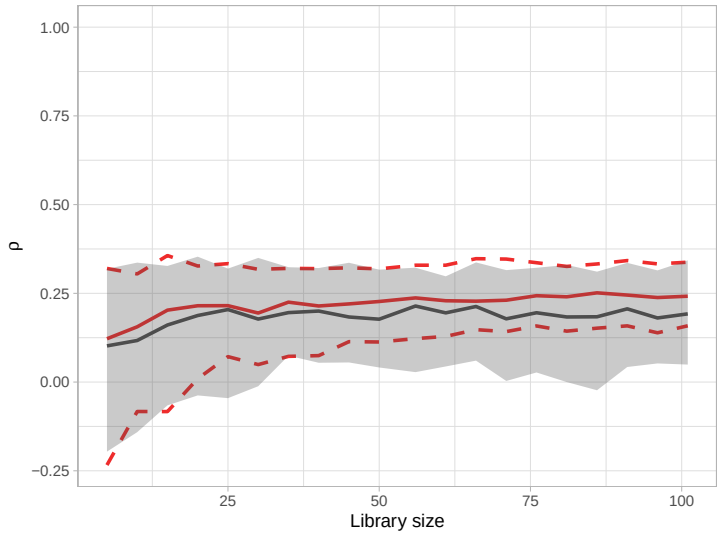


**Figure 32:** CCM from productivity to SST without convergence for the stock CALSCORPSCAL, with the forecasting skill of the cross-mapping depending on the library size L. The red curves represents the CCM applied on the original data (median of the 100 bootstraps for each L in solid line, and 5-95% quantiles in dashline). The grey curve represents the median of the forecasting skills for the 100 random shuffles (null model). The grey ribbon represents the 5-95% quantiles of the forecasting skills for the 100 random shuffles.

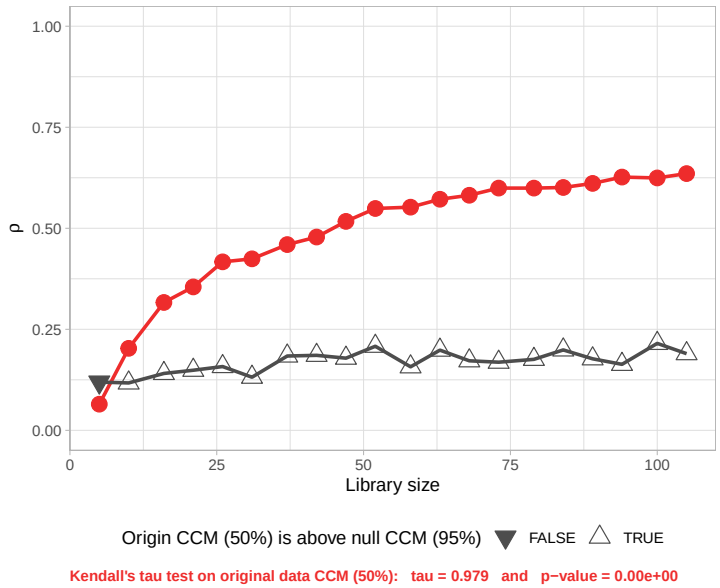


**Figure 33:** Tests in the CCM to assess causality, for the stock MORWONGESE in productivity cross-mapped to SST. The red curve represents the median of bootstraps on the original data. The grey curve is the 95% quantile of the null model. The Mann-Kendall test applied to the median of the bootstraps on original data is significant here.

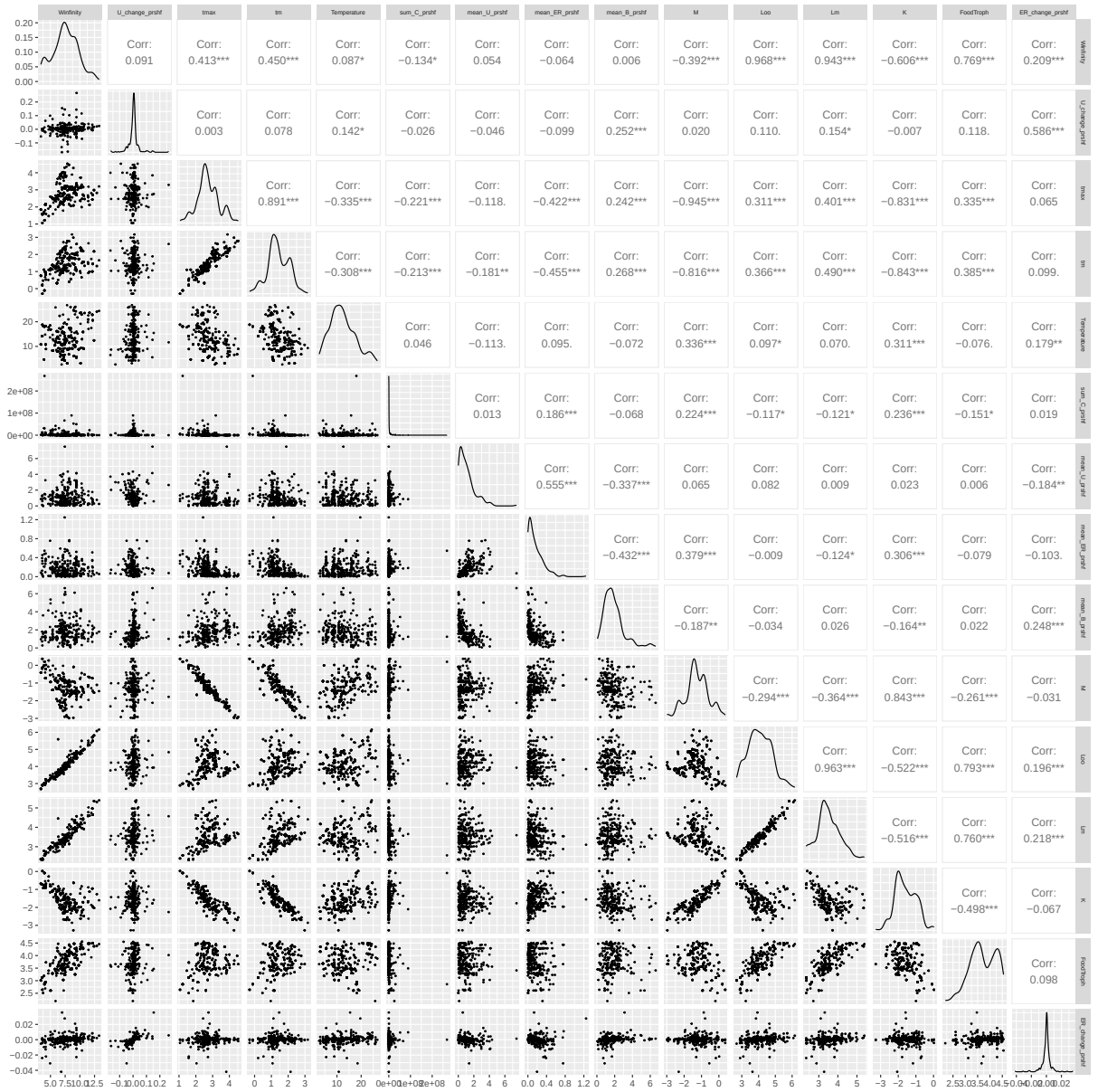


**Figure 34:** Pair plots of the functional traits and management variables used in the analysis

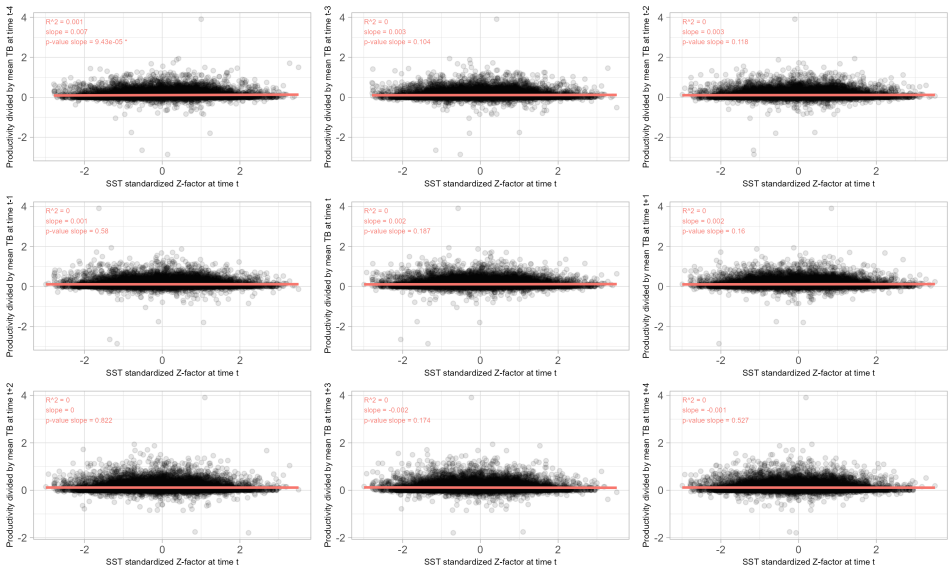


**Figure 35:** Linear models between $\mathrm{Prod}(t+l)$ and $\mathrm{SST}(t)$ for lags $l$ between -4 and 4

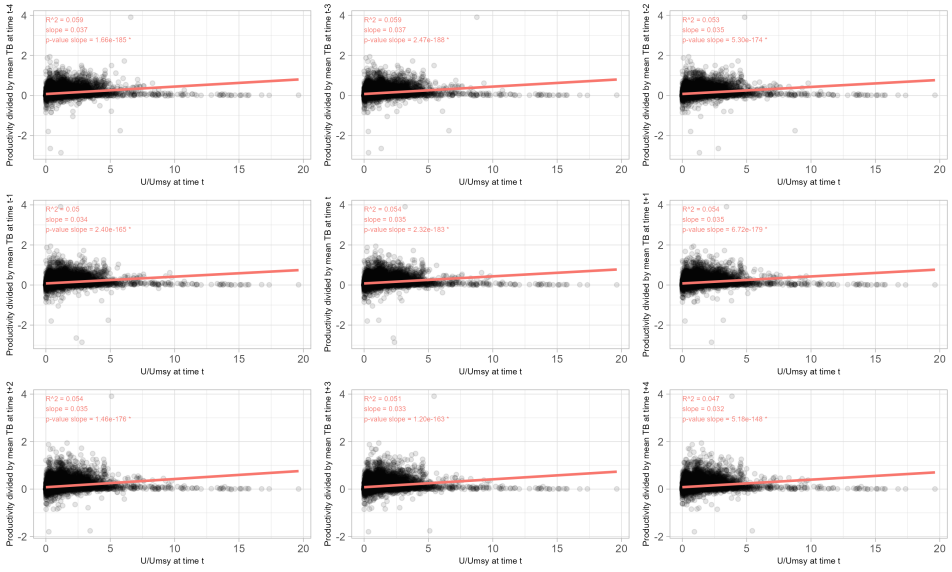


**Figure 36:** Linear models between $\mathrm{Prod}(t+l)$ and $\mathrm{U}(t)$ for lags $l$ between -4 and 4

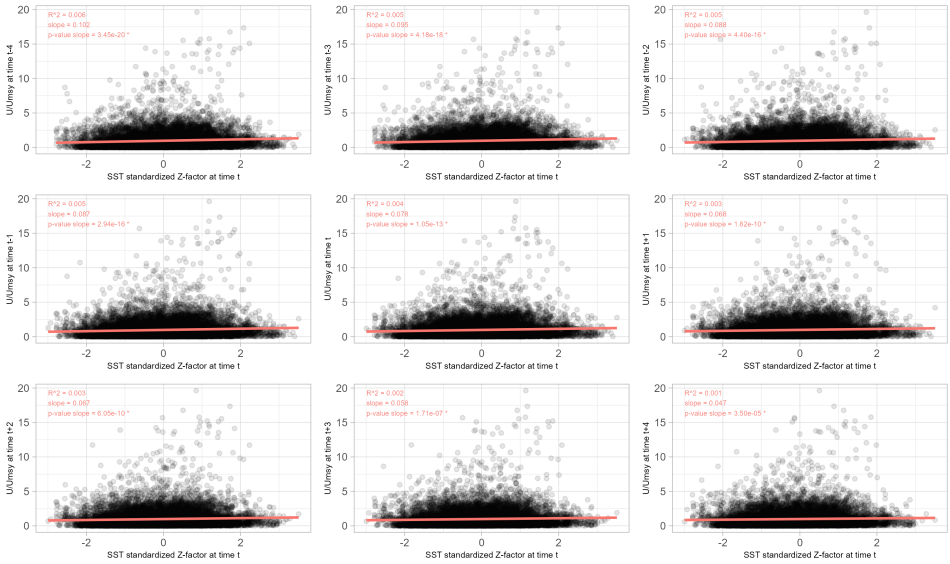


**Figure 37:** Linear models between $\mathrm{U}(t+l)$ and $\mathrm{SST}(t)$ for lags $l$ between -4 and 4

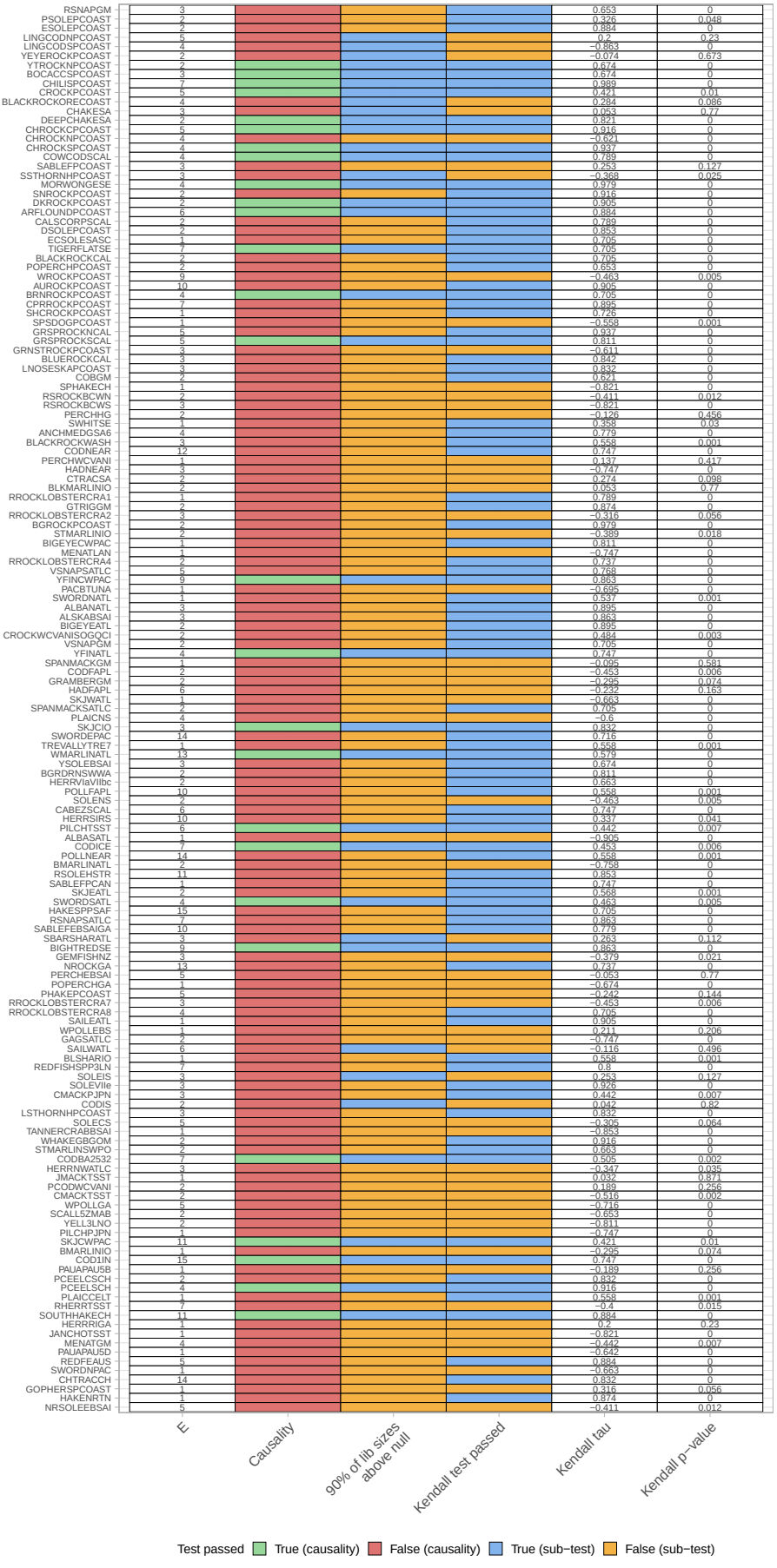


**Figure 38:** CCM all assessment (prod xmap SST)

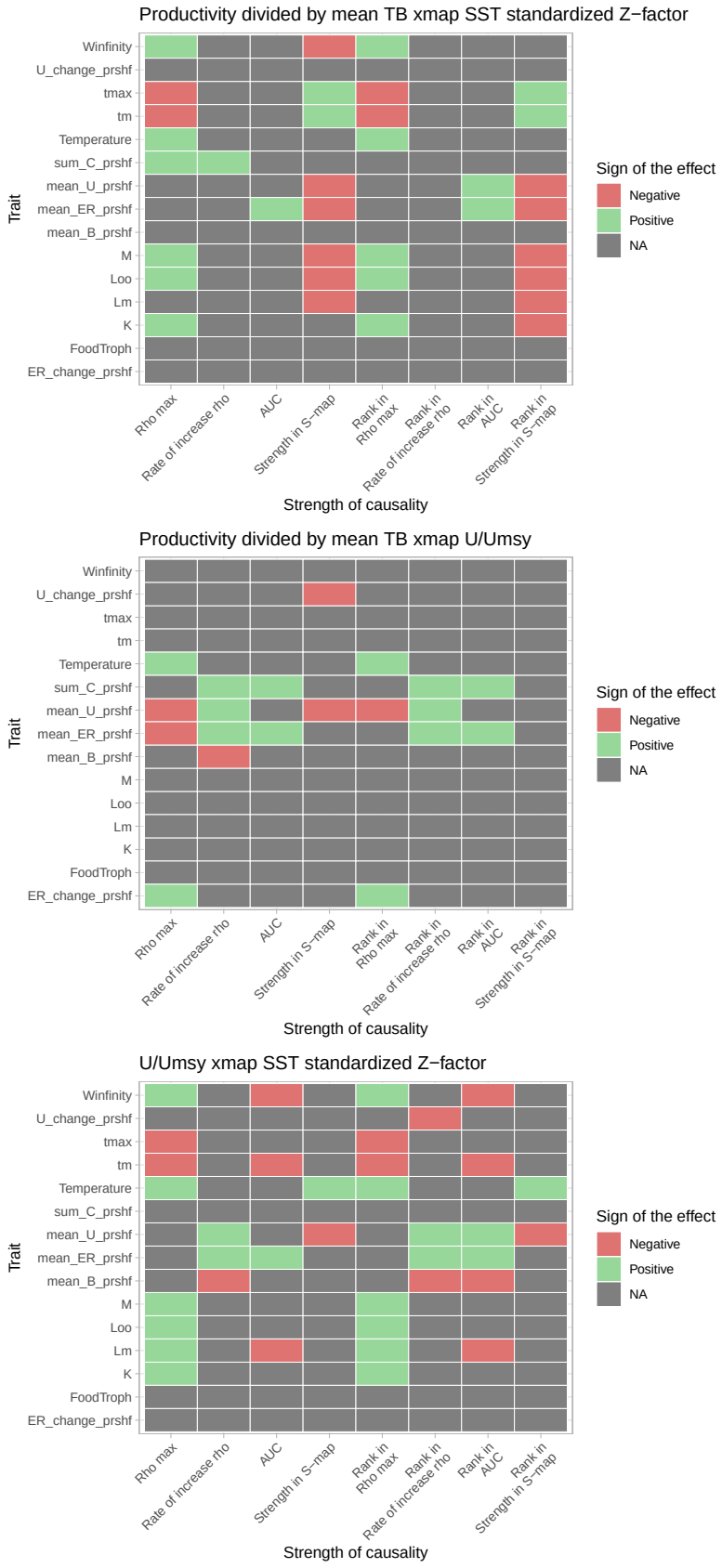


**Figure 39:** Summary of the effects of traits and management variables on the confidence or the strength of the causality (value or rank). Significance is evaluated when the p-value of the test of nullity of the slope is below 5%. If the relationship is significant, the sign is defined from the sign of the slope. If not, the is noted `NA`. Top: SST causing productivity, middle: harvest rate causing productivity, bottom: SST causing harvest rate.

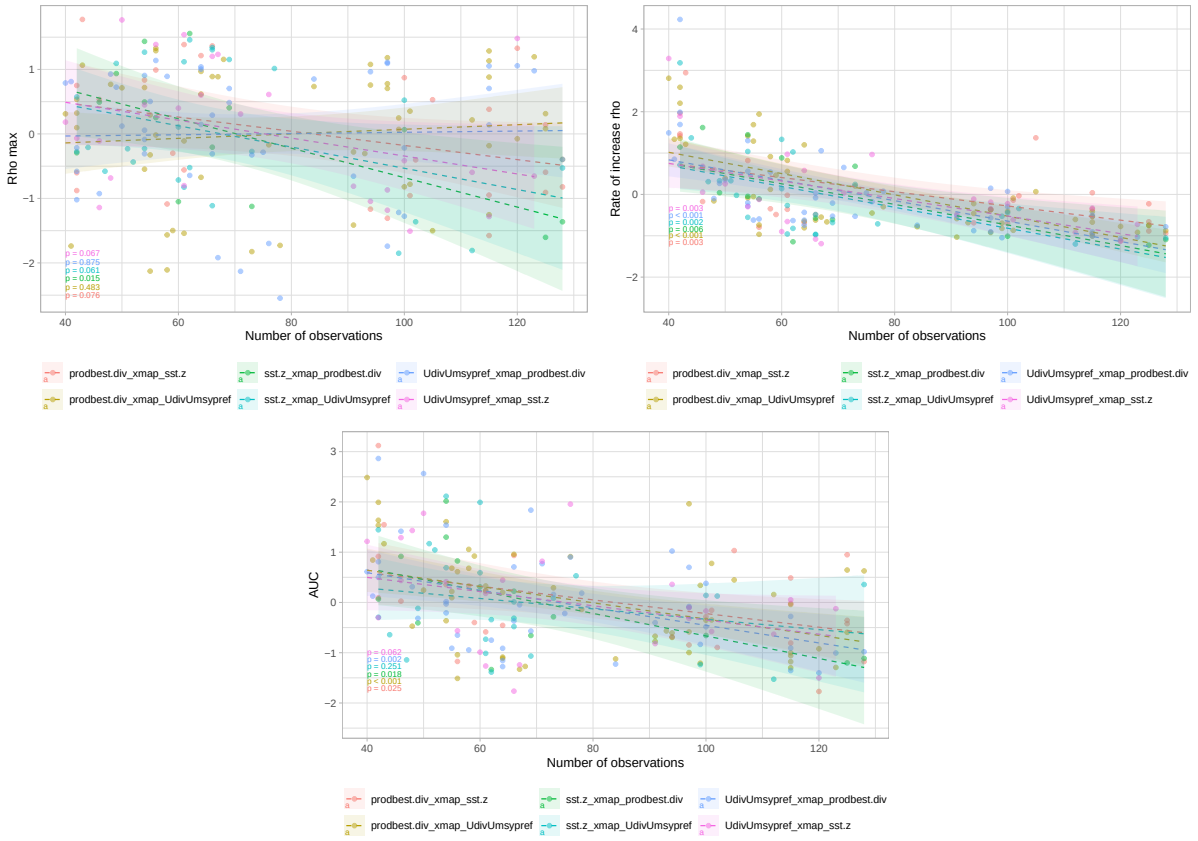


**Figure 40:** Effect of length of time series on the confidence in the causality. The colors represent the pairs of variables tested in the CCM.

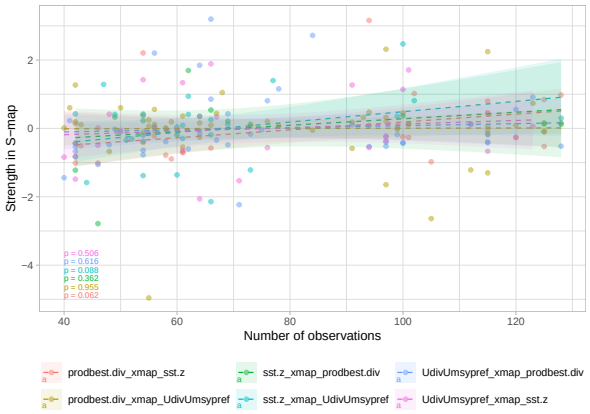


**Figure 41:** Effect of length of time series on the strength of causality. The colors represent the pairs of variables tested in the CCM.

# List of Figures


1 Main statistical methods for assessing quasi-causality . . . . . 4
2 Embedding and manifold approximation used in the CCM for the Lorenz attractor . . . . . 11
3 Definition of the surplus of productivity . . . . . 13
4 Sea Surface Temperature (SST) data with the boundary of the MORWONGESE stock . . . . . 14
5 Example of the three time series for the stock MORWONGESE. . . . . 15
6 Time series of each variable for all stocks . . . . . 16
7 Visualization of the simplex projection (productivity - stock MORWONGESE) 18
8 Forecasting skill in the simplex projection depending on the embedding dimension for the productivity of the stock MORWONGESE . . . . . 19
9 Forecasting skill in the simplex projection depending on the embedding dimension for the productivity for all the stocks . . . . . 19
10 Forecasting skill in the simplex projection at the optimal embedding dimension for the productivity for each stock . . . . . 21
11 Forecasting skill in the simplex projection depending on the time horizon of prediction for the productivity of the stock MORWONGESE . . . . . 22
12 Forecasting skill in the S-map at optimal $E$ as a function of the nonlinearity parameter $\theta$ (productivity - stock MORWONGESE) . . . . . 23
13 Forecasting skill in the S-map depending on the nonlinearity parameter $\theta$ and $E$ (productivity - stock MORWONGESE) . . . . . 24
14 Example of embedding space of 3 dimensions of productivity for the stock MORWONGESE . . . . . 25
15 Prediction of SST from productivity in the CCM (optimal $E = 4$) for library sizes $L = 5$ (top), $L = 37$ (middle), and $L = 105$ (bottom) . . . . . 27
16 Convergence for the CCM from productivity to SST for the MORWONGESE stock . . . . . 28
17 Spearman correlation between pairs of variables . . . . . 34
18 Histogram of optimal embedding dimensions $E$ . . . . . 35
19 Forecasting skill as a function of the time horizon of prediction for all stocks 36
20 Forecasting skill depending on the nonlinearity parameter $\theta$ for all stocks . 37
21 Histograms of the optimal nonlinearity parameters $\theta$ . . . . . 38
22 Causality detection from tests on the CCM . . . . . 39
23 Metrics of confidence in causality and strength of causality . . . . . 40

24 Boxplot of the strength of causality for each pair of variables . . . . . 41
25 Relationships between traits and confidence in causality . . . . . 42
26 Relationships between traits and strength of causality in S-map . . . . . 43
27 Effect of time series length on forecasting skill or on the optimal embedding dimension . . . . . 47
28 Time series length depending on causality assessment . . . . . 47
29 Duration of the time series for each stock used from RAMLDB . . . . . 54
30 Autocorrelations within the time series of productivity (upper left), SST (upper right) and harvest rate(bottom) . . . . . 55
31 CCM prediction vs observed for the stock MORWONGESE in productivity cross-mapped with temperature with the libsize of 5, 37 and 105 . . . . . 55
32 CCM from productivity to SST without convergence for the stock CALSCORP-SCAL . . . . . 56
33 Tests in the CCM to assess causality, for the stock MORWONGESE in productivity cross-mapped to SST . . . . . 56
34 Pair plots of the functional traits and management variables used in the analysis . . . . . 57
35 Linear models between Prod$(t+l)$ and SST$(t)$ for lags $l$ between -4 and 4 . 58
36 Linear models between Prod$(t+l)$ and U$(t)$ for lags $l$ between -4 and 4 . . 58
37 Linear models between U$(t+l)$ and SST$(t)$ for lags $l$ between -4 and 4 . . 59
38 CCM all assessment (prod xmap SST) . . . . . 60
39 Summary of the effects of traits and management variables on the confidence or the strength of the causality . . . . . 61
40 Effect of length of time series on the confidence in the causality . . . . . 62
41 Effect of length of time series on the strength of causality . . . . . 62